


## RESEARCH ARTICLE

# Creld2 function during unfolded protein response is essential for liver metabolism homeostasis

Paul Kern<sup>1,2</sup> | Nora R. Balzer<sup>1</sup> | Nelli Blank<sup>1</sup> | Cornelia Cygon<sup>1</sup> | Klaus Wunderling<sup>3</sup> | Franziska Bender<sup>2</sup> | Alex Frolov<sup>1</sup> | Jan-Peter Sowa<sup>4,5</sup> | Lorenzo Bonaguro<sup>6,7</sup> | Thomas Ulas<sup>6,7</sup> | Mirka Homrich<sup>8</sup> | Eva Kiermaier<sup>8</sup> | Christoph Thiele<sup>3</sup> | Joachim L. Schultze<sup>6,7,9</sup> | Ali Canbay<sup>4,5</sup> | Reinhard Bauer<sup>2</sup> | Elvira Mass<sup>1</sup> 

<sup>1</sup>Developmental Biology of the Immune System, Life & Medical Sciences (LIMES) Institute, University of Bonn, Bonn, Germany

<sup>2</sup>Developmental Genetics & Molecular Physiology, Life & Medical Sciences (LIMES) Institute, University of Bonn, Bonn, Germany

<sup>3</sup>Biochemistry & Cell Biology of Lipids, Life & Medical Sciences (LIMES) Institute, University of Bonn, Bonn, Germany

<sup>4</sup>Department of Gastroenterology, Hepatology and Infectious Diseases, University Hospital Magdeburg, Magdeburg, Germany

<sup>5</sup>Department of Medicine, Ruhr University Bochum, University Hospital Knappschaftskrankenhaus Bochum, Bochum, Germany

<sup>6</sup>Genomics and Immunoregulation, Life & Medical Sciences (LIMES) Institute, University of Bonn, Bonn, Germany

<sup>7</sup>Platform for Single Cell Genomics and Epigenomics at the Deutsche Zentrum für Neurodegenerative Erkrankungen (DZNE), University of Bonn, Bonn, Germany

<sup>8</sup>Immune and Tumor Biology, Life & Medical Sciences (LIMES) Institute, University of Bonn, Bonn, Germany

<sup>9</sup>Systems Medicine, Deutsches Zentrum für Neurodegenerative Erkrankungen (DZNE), Bonn, Germany

## Correspondence

Elvira Mass, Developmental Biology of the Immune System, Life & Medical Sciences (LIMES) Institute, University of Bonn, 53115 Bonn, Germany.  
Email: emass@uni-bonn.de

## Funding information

Fritz Thyssen Stiftung (Fritz Thyssen Foundation), Grant/Award Number: Az.10.18.2.029MN; Deutsche Forschungsgemeinschaft (DFG), Grant/Award Number: EXC2151-390873048 and CA267/14-1; Bundesministerium für Bildung und Forschung (BMBF), Grant/Award Number: DietBB (01EA1809A); Daimler und

## Abstract

The unfolded protein response (UPR) is associated with hepatic metabolic function, yet it is not well understood how endoplasmic reticulum (ER) disturbance might influence metabolic homeostasis. Here, we describe the physiological function of Cysteine-rich with EGF-like domains 2 (Creld2), previously characterized as a downstream target of the ER-stress signal transducer Atf6. To this end, we generated *Creld2*-deficient mice and induced UPR by injection of tunicamycin. *Creld2* augments protein folding and creates an interlink between the UPR axes through its interaction with proteins involved in the cellular stress response. Thereby, *Creld2* promotes tolerance to ER stress and recovery from acute stress. *Creld2*-deficiency leads to a dysregulated UPR and causes the development of hepatic steatosis during ER stress conditions. Moreover, *Creld2*-dependent

**Abbreviations:** ALT, alanine aminotransferase; Atf6, activating transcription factor 6; CD, control diet; Chop, CAAT/enhancer-binding protein (C/EBP) homologous protein; *Creld2*, cysteine-rich with EGF-like domains 2; eIF2 $\alpha$ , translation initiation factor 2 $\alpha$ ; ER, endoplasmic reticulum; ERAD, ER-associated protein degradation; Gadd34, DNA-damage-inducible protein 34; Grp78, glucose-regulated protein 78; HFD, high-fat diet; HOMA-IR, homeostatic model assessment of insulin resistance; Ire1, inositol requiring enzyme 1; MGT, Masson-Goldner trichrome; NAFLD, non-alcoholic fatty liver disease; NASH, non-alcoholic steatohepatitis; Perk, protein kinase RNA-activated (PKR)-like ER kinase; Tm, tunicamycin; UPR, unfolded protein response; Xbp1, X-box binding protein 1.

This is an open access article under the terms of the Creative Commons Attribution-NonCommercial-NoDerivs License, which permits use and distribution in any medium, provided the original work is properly cited, the use is non-commercial and no modifications or adaptations are made.

© 2021 The Authors. *The FASEB Journal* published by Wiley Periodicals LLC on behalf of Federation of American Societies for Experimental Biology

Benz Stiftung (Daimler and Benz Foundation), Grant/Award Number: 32-058/18

enhancement of the UPR assists in the regulation of energy expenditure. Furthermore, we observed a sex dimorphism in human and mouse livers with only male patients showing an accumulation of CRELD2 protein during the progression from non-alcoholic fatty liver disease to non-alcoholic steatohepatitis and only male *Creld2*-deficient mice developing hepatic steatosis upon aging. These results reveal a *Creld2* function at the intersection between UPR and metabolic homeostasis and suggest a mechanism in which chronic ER stress underlies fatty liver disease in males.

#### KEYWORDS

*Creld2*, ER stress, liver steatosis, NASH, UPR

## 1 | INTRODUCTION

The Cysteine-rich with EGF-like domains (*Creld*) protein family consists of two members—*Creld1* and *Creld2*—and is highly conserved across species.<sup>1,2</sup> The domain structure between these proteins is almost identical, with the only difference of transmembrane domains being present in *Creld1* but lacking in *Creld2*.<sup>3</sup> This leads to their distinct localization and functions within a cell. *Creld1* is found anchored in the plasma membrane facing the extracellular matrix.<sup>1,4</sup> We previously characterized the function of *Creld1* as being essential for heart development and immune cell function in mice.<sup>4–6</sup> In contrast, *Creld2* is localized predominantly within the endoplasmic reticulum (ER) and can be secreted.<sup>3,7,8</sup> Indeed, *Creld2* has been suggested as a biomarker in human body fluids for molecular phenotyping of pathophysiologies such as kidney disease<sup>9</sup> and prosthetic joint infections.<sup>10</sup> Several in vitro studies have identified *Creld2* initially as an ER-stress inducible gene, whose expression is dependent on the activity of ER stress sensor activating transcription factor 6 (*Atf6*).<sup>11,12</sup> However, also the activity of the other ER stress sensors inositol requiring enzyme 1 (*Ire1*) and protein kinase RNA-activated (*PKR*)-like ER kinase (*Perk*) can induce *Creld2* expression.<sup>8,13,14</sup>

ER stress is characterized by an accumulation of mis- and/or unfolded proteins in the ER lumen. Consequently, cells activate the unfolded protein response (UPR), a network of signaling pathways that collectively aims at decreasing ER protein load by broad inhibition of protein synthesis. At the same time, UPR promotes the activation and production of proteins that increase the protein folding capacity and protein degradation. The latter include chaperones, shuttling proteins that promote the secretion of proteins out of the ER, and ER-associated protein degradation (ERAD) components.<sup>15,16</sup> The ER luminal domains of the ER stress sensors are bound and thereby inactivated by the chaperone Grp78 (glucose-regulated

protein 78, also known as heat shock protein A5 (*Hspa5*)). Upon ER stress, Grp78 is sequestered by the accumulation of proteins in the ER lumen, causing the activation of the three sensors. *Perk* dimerizes and is activated by trans-autophosphorylation of its kinase domains, leading to translational inhibition through eIF2 $\alpha$  phosphorylation. This directly enhances the translation of DNA-damage-inducible protein 34 (*Gadd34*) and CAAT/enhancer-binding protein (*C/EBP*) homologous protein (*Chop*). *Gadd34* serves as a feedback loop to dephosphorylate eIF2 $\alpha$ , thereby promoting the recovery from translational inhibition. In contrast, prolonged *Chop* expression may trigger cell death due to unresolved ER stress. The kinase *Ire1* is auto-phosphorylated, which results in splicing of the *X-box binding protein 1* (*sXbp1*) mRNA. The active transcription factor *sXbp1* then induces the transcription of chaperones and ERAD pathway components. ER-membrane bound *Atf6* is proteolytically cleaved and translocates to the nucleus, where it activates target genes, including ERAD components, chaperones, and lipid metabolism genes.<sup>17</sup>

*Creld2* has been proposed to possess protein disulfide isomerase (*PDI*)-like activity within this complex ER-stress response, which is essential for correct disulfide-bond formation and rearrangement when incorrect bonds are made during UPR.<sup>18</sup> *Creld2* acts as a chaperone during skeletal development, promoting the transport of receptor low-density lipoprotein receptor-related protein 1 (*LRP1*) to the cell surface.<sup>19</sup> Thus, evidence is mounting that *Creld2* plays a key role during homeostasis and UPR-associated disease progression. However, the physiological role of *Creld2* in secretory organs during homeostasis and after ER-stress induction has not been addressed.

The liver frequently serves as a model tissue to investigate ER stress. Previous studies demonstrate that induction of ER stress leads to hepatic steatosis through the direct and indirect regulation of lipid metabolism.<sup>20–22</sup> On the contrary, in genetic and dietary models of obesity,

a link between hepatic stress and insulin resistance has been established,<sup>23–26</sup> suggesting that the accumulation of lipids within hepatocytes and the resulting hepatocellular damage is linked to dysfunction of the ER. Therefore, the arrow of causality between the onset of hepatosteatosis and chronic UPR remains unclear in many liver pathologies characterized by the dysregulation of metabolic and ER homeostasis, e.g., in non-alcoholic steatohepatitis (NASH).

*Atf6* knockout mice do not exhibit developmental defects or any obvious phenotypes at steady-state but show an abrogated response to ER stress upon challenge with the ER stressor tunicamycin (Tm), which macroscopically manifests in the development of liver steatosis.<sup>21,27</sup> Furthermore, *Atf6* regulates physiological responses under diet-induced obesity,<sup>28</sup> suggesting the UPR acting upstream of hepatosteatosis.

To address the function of *Creld2* within the UPR and its possible role in hepatic pathophysiology, we generated a *Creld2* knockout mouse and characterized its role during ER stress challenge and diet-induced obesity in the liver. We show that *Creld2*-deficiency promotes the development of liver steatosis in aged male mice or when burdened with ER stress, while lack of *Creld2* ameliorates diet-induced hepatosteatosis. Furthermore, we identify *Creld2* protein interaction partners that are involved in ER-stress release, thereby placing *Creld2* functionally into the cellular stress response of a cell in vivo. The conserved function of *Creld2* across species is supported by the accumulation of CRELD2 in male patients with NASH.

## 2 | MATERIALS AND METHODS

### 2.1 | Mouse work

For the generation of a conventional *Creld2*<sup>eGFP/eGFP</sup> mouse, the open reading frame (ORF) of the *Creld2* gene was replaced by an enhanced green fluorescent protein (eGFP) and a neomycin resistance cassette (neoR) flanked by two FRT sites via homologous recombination. False-positive ES cell clones were excluded by a diphtheria toxin A (DTA) cassette, which was introduced after the 3' homologous region of the targeting vector. Positive ES cell clones were selected by PCR against the neoR cassette and confirmed by Southern blot via an internal and 5' external probe. Heterozygous *Creld2*<sup>WT/eGFP/neo</sup> offspring from blastocyst injections of positive ES cell clones were crossed with mice ubiquitously expressing FLP recombinase for excision of the neoR cassette. neoR deletion was confirmed by PCR. Mice were provided with standard chow and autoclaved water ad libitum. Genotyping

primers: *Creld2* wt genotype fw 5'-CCTGAGCTGTCCTTAGAAAGTTGCTAG-3', *Creld2* ko genotype fw 5'-GCCCCACAACCACTACCTGAGC-3', *Creld2* genotype rev 5'-GGGGTTCATGTCCATGGGCCAC-3'.

To induce hepatic UPR, 8- to 9-week-old male mice were administered with Tm (1 mg/kg in 150 mM sucrose) or a vehicle control sucrose solution (150 mM) via i.p. injection and sacrificed after 48 h.

For HFD experiments, male mice received standard chow until six weeks of age. Afterward, standard chow was replaced by a control diet (CD; metabolizable energy: 62% from carbohydrates, 11% from fat, 27% from protein; ssniff EF D12450B\* mod. LS) for two weeks prior to the beginning of the experiment. Subsequently, 8-week-old mice were either fed with CD or HFD (metabolizable energy: 22% from carbohydrates, 54% from fat, 24% from protein; ssniff EF acc. D12492 (I) mod.) for 12 weeks or mice were kept on HFD for eight weeks and CD for four weeks (HFD > CD). Mice were weighed once a week. To determine the Homeostatic model assessment of insulin resistance (HOMA-IR),<sup>29</sup> mice were fasted for 6 h, and blood was drawn from 8-week-old mice at the beginning of the feeding period and from mice being fed CD or HFD for eight weeks. Blood samples were analyzed for blood glucose using a glucose meter (Accu-Chek, Aviva) and blood serum insulin levels (Mouse Insulin Elisa kit, Thermo Scientific) according to the manufacturers' instructions. HOMA-IR indices were calculated using the formula: (Glucose (mg/ml) × Insulin (μU/ml))/405.

All mice were kept under standard SPF housing conditions with a 12 h dark/light cycle. All animal experiments were approved by the government under the license 84-02.04.2017.A335.

### 2.2 | Histological stainings

For paraffin stains, tissues were fixed in 4% PFA (Thermo Scientific). After fixation, tissues were dehydrated, paraffin-embedded, and cut at a thickness of 5 μm. Subsequently, sections were deparaffinized, rehydrated, and stained with Hematoxylin followed by Eosin (VWR), PAS (Roth), or MGT (Merck) according to the manufacturer's protocol. After dehydration, tissues were mounted in Entellan. For Cryo-embedded (Tissue-Tek, Sakura) tissue stains, sections were fixed in 4% PFA and stained with freshly prepared oil-red-O (Sigma-Aldrich) working solution according to the manufacturer's instructions, followed by mounting in Kaiser's glycerol gelatine (Merck). Quantitative analyses of PAS, MGT, and ORO stainings were done using ImageJ2 software. Scripts for quantifications are provided upon reasonable request.

## 2.3 | Bone marrow-derived macrophage (BMDM) isolation and LPS treatment

Femur and tibia of sacrificed mice were dissected and flushed with PBS using a 26G needle and cultured in DMEM (Invitrogen) medium supplied with 10% FCS (Pan Biotech), 1% Pen-Strep (10 000 U/ml; Thermo Scientific), 20% L929 cell medium supernatant for 6 days. Subsequently, differentiated BMDMs were stimulated with LPS (200 ng/ml; from *Escherichia coli* O111:B4; Sigma-Aldrich) for 4–8 h.

## 2.4 | Kupffer cell flow cytometry

Livers were harvested and incubated in digestion buffer (PBS, 1 mg/ml collagenase D (Roche), 100 U/ml DNase I (Sigma-Aldrich), 2.4 mg/ml dispase (Invitrogen), 3% FCS (Invitrogen)) at 37°C for 30 min prior to mechanical disruption by straining through a 100 µm cell filter. Cell suspensions were centrifuged at 50 g for 3 min to sediment hepatocytes, supernatants were recovered, centrifuged at 320 g for 7 min and incubated in FACS buffer (PBS, 0.5% BSA, 2 mM EDTA) containing anti-CD16/32 (1:100 dilution), 5% normal mouse, 5% normal rabbit and 5% normal rat serum for 15 min at 4°C. After the incubation, cells were immunostained with antibody mixtures (CD45-APC/Cy7 (30-F100), CD11b-PECy7 (M1/70), F4/80-BV421 (BM8), Tim4-AF647 (RMT4-54) (all from Biolegend)) for 30 min at 4°C. Single live cells were selected by excluding dead cells (Hoechst 33 258, 1:10.000), gating on side (SSC-A) and forward scatter (FSC-A) and excluding doublets using forward scatter width (FSC-W) against FSC-A. Kupffer cells were identified by gating on CD45<sup>+</sup>, CD11b<sup>low</sup>, F4/80<sup>+</sup>Tim4<sup>+</sup> cells.

## 2.5 | qPCR

RNA was isolated using the Nucleospin RNA II kit (Macherey & Nagel) according to the manufacturer's instructions and reverse transcribed into cDNA using the QantiTect reverse transcription kit (Qiagen) according to the manufacturer's instructions. For qRT-PCR reactions, primer pairs (see Table S1) were mixed with cDNA and iQ SYBR<sup>®</sup>Green Supermix (Bio-Rad), and qRT-PCR was run on an iQs Real-Time PCR Detection System (Bio-Rad). Genes of interest were normalized to the reference genes *Ppia* (peptidylprolyl isomerase A) and *Hprt* (hypoxanthine-guanine phosphoribosyltransferase) for calculation of the Delta-Delta Cq value by the inherent qRT-PCR evaluation software CFX manager (Bio-Rad). For human *CRELD2* gene expression levels analysis, *HPRT* was used as a

reference gene. Relative gene expression was calculated from the threshold cycles in relation to the reference gene and controls without NAFLD. Reactions were performed on a CFX96 Touch qPCR System (Bio-Rad). Gene expression data (housekeeper normalized delta delta Cq values) were scaled to individual genes separately for each gender before averaging and plotting heatmaps using the pheatmap R-package to represent qRT-PCR as heatmaps.

## 2.6 | Library preparation for RNA sequencing

mRNA was converted into libraries of double-stranded cDNA molecules as a template for high-throughput sequencing following the SMART-Seq2 protocol.<sup>30</sup> Shortly, mRNA was primed for SMART reverse transcription from 5 ng of total RNA using poly-T oligos. cDNA was pre-amplified by SMART ISPCR. Fragmentation was performed using the Illumina Nextera XT kit, followed by PCR amplification and indexing. Size-selection and purification of library fragments with preferentially 300–400 bp in length were performed using SPRIbeads (Beckman-Coulter). The size distribution of cDNA libraries was measured using the Agilent high sensitivity D5000 assay on a TapeStation 4200 system (Agilent). cDNA libraries were quantified using a Qubit high sensitivity dsDNA assay. 75 bp single-end sequencing was performed on a NextSeq500 system using High Output v2.5 chemistry. Base calling from base call files, alignment to the *Mus musculus* reference genome mm10 from UCSC, and file conversion to fastq files were achieved by Illumina standard pipeline scripts (STAR version, bcl2fastq2 v.2.20).

## 2.7 | RNA sequencing analysis

Kallisto pseudo-alignment<sup>31</sup> was used to quantify abundances of transcripts—read counts—from the bulk RNA-seq data. The kallisto read counts were used as input to DESeq2<sup>32</sup> to calculate normalized signal and differential gene expression. Genes are excluded from the analysis where the total read count of all samples is less than 10. This pre-filtering step removes genes in which there are very few reads to reduce the memory size and increase the speed of the calculation. The diet and drug-induced ER-stress dataset then comprised 25308 and 23985 genes, respectively. DESeq Dataset (dds) was created to store the read counts, and the intermediate estimated quantities with a merged design formula consist of genotype (*Creld2*<sup>WT/WT</sup> or *Creld2*<sup>eGFP/eGFP</sup>) and condition (dietary or pharmacological). Regularized log transformations (rlog) were used



for the downstream analysis (clustering). Rlog produces transformed data on the log2 scale, which has been normalized with respect to library size. Unwanted surrogate variables were estimated and modeled via Surrogate Variable Analysis (SVA)<sup>33</sup> using the “leek” method. In the diet-related experiment, four surrogate variables (SV) were identified and modeled. For the pharmacologically induced dataset, three SVs were identified and modeled. For DE gene analysis of CD versus HFD conditions, the lfc threshold was set to 1.32, and the *p*-value threshold to .05. The top 5000 variable genes were selected and used as an input for co-expressional network analysis using CoCena<sup>2</sup> (<https://github.com/UlasThomas/CoCena2>). Pearson correlation analysis was performed with a correlational significance measure of *p* < .05. The correlation coefficient cut-off was .706 for the diet-induced dataset and .659 for the pharmacologically-induced dataset. Based on a greedy approach, the Louvain community detecting algorithm<sup>34</sup> was used to cluster the genes of the diet-induced dataset based on expression patterns between the different conditions. For the pharmacologically-induced dataset, the infomap community detection algorithm<sup>35</sup> was used. Clustering was repeated 100 times. The minimal number of genes per cluster was set to 50. Gene set enrichment analysis (GSEA) was performed on all cluster genes using the following knowledge bases: Hallmark, Reactome, GO, KEGG, and DO. ClusterProfiler package<sup>36</sup> was used for all GSEAs using default options with the respective correlation coefficient cut-off for each dataset. The prior mechanisms associated with the Co-Cena clusters were manually selected from the GSEA results based on prior knowledge.

## 2.8 | Thin-layer chromatography

Total lipids were extracted as described by Bligh and Dyer.<sup>37</sup> Livers were homogenized in ice-cold H<sub>2</sub>O (50 mg wet weight/ml) in a Precellys homogenizer (Peqlab Biotechnology, Germany). 3 ml of chloroform/methanol 1:2 (v:v) were added to 800 µl homogenate and vortexed. 1 ml of chloroform was added to the mixture and vortexed before adding 1 ml H<sub>2</sub>O. The mixture was thoroughly vortexed and centrifuged at 1000 g for 5 min at RT, and the lower solvent phase was recovered. The same volumes of the solvent phase were evaporated under nitrogen, and lipids were resuspended in 100 µl of chloroform/methanol 1:1 (v:v) (Merck). Lipid extracts corresponding to 1 mg wet liver weight were applied onto HPTLC silica gel 60 plates (10 × 20 cm; Merck), and plates were developed in *n*-hexane/diethyl ether/acetic acid 70:30:5 (v/v/v) (Merck, Roth) in a developing chamber (CAMAG, Switzerland). Dried plates were soaked in charring solution (copper

sulfate (CuSO<sub>4</sub>) 10% and phosphoric acid (H<sub>2</sub>PO<sub>4</sub>) 8% (Roth)) and heated to 180°C for 5–10 min for lipid visualization.

## 2.9 | Lipid mass spectrometry

Livers were homogenized in ddH<sub>2</sub>O at a concentration of 20 mg (wet weight)/ml using a Precellys homogenizer (Peqlab Biotechnology). For lipid extraction, 50 µl of the homogenate were added to 500 µl of extraction mix (CHCl<sub>3</sub>/MeOH 1/5 containing internal standards: 210 pmol PE(31:1), 396 pmol PC(31:1), 98 pmol PS(31:1), 84 pmol PI(34:0), 56 pmol PA(31:1), 51 pmol PG (28:0), 28 pmol CL(56:0), 39 pmol LPA (17:0), 35 pmol LPC(17:1), 38 pmol LPE (17:0), 32 pmol Cer(17:0), 99 pmol SM(17:0), 55 pmol GlcCer(12:0), 14 pmol GM3 (18:0-D3), 359 pmol TG(47:1), 111 pmol CE(17:1), 64 pmol DG(31:1), 103 pmol MG(17:1), 724 pmol Chol(d6), 45 pmol Car(15:0)) were added and the sample sonicated for 2 min followed by centrifugation at 20 000 g for 2 min. The supernatant was collected into a new tube, and 200 µl chloroform and 800 µl 1% AcOH in water were added, the sample briefly shaken and centrifuged for 2 min at 20 000 g. The upper aqueous phase was removed, and the entire lower phase was transferred into a new tube and evaporated in a speed vac (45°C, 10 min). Spray buffer (500 µl of 8/5/1 2-propanol/MeOH/water, 10 mM ammonium acetate) was added, the sample sonicated for 5 min, and infused at 10 µl/min into a Thermo Q Exactive Plus spectrometer equipped with the HESI II ion source for shotgun lipidomics. MS1 spectra (resolution 280 000) were recorded in 100 *m/z* windows from 250 to 1200 *m/z* (pos.) and 200–1700 *m/z* (neg.) followed by recording MS/MS spectra (res. 70 000) by data independent acquisition in 1 *m/z* windows from 200 to 1200 (pos.) and 200 to 1700 (neg.) *m/z*. Raw files were converted to .mzml files and imported into and analyzed by LipidXplorer software using custom mfql files to identify sample lipids and internal standards. For further data processing, absolute amounts were calculated using the internal standard intensities followed by the calculation of mol% of the identified lipids.

## 2.10 | Tandem affinity purification of tagged Creld2

HEK293 cells were electroporated with plasmid DNA pcDNA3.1/Zeo(+) (Addgene) containing only the Strep-Flag (SF)-tag (mock), N-terminally tagged Creld2 (FS-C2) where the tag was integrated after the signal peptide or C-terminally tagged Creld2 (C2-SF). Gene blocks were used to clone the constructs (see Table S2). Primer used

for cloning: NheI-Kozak-mC2-SF-tag fw 5'-CTAGCTAGC GCCACCATGCACCTGCTGCTTGCA-3', 5'-Crel2-KpnI TATGGTACCTCACAAATCCTCACGGGAGGG-3', KpnI-Flagrev5'-TAGGGTACCTCACTTGTCGTCGTC-3', NheI-SF-tag fw 5'-CTAGCTAGCATGGGTGGAGGTTCT GGA-3', KpnI-SF-tag rev 5'-GGAGCTCTGGATGGTACC TCACTTGTC-3'.

Plasmids comprised a zeocin resistance cassette for selection. Cells transiently expressing C2-SF were harvested 72 h post electroporation for tandem-affinity-purification (TAP). For the generation of stably expressing cell lines, plasmid DNA was linearized prior to electroporation and selected for stable expression by Zeocin (200 µg/ml) resistance for four weeks with validation of construct expression via immunoblotting against Crel2 and Flag (data not shown). For TAP cells were incubated on ice in freshly prepared, ice-cold TAP-lysis buffer (1x Complete protease inhibitor (Roche), 1x Phosphate inhibitor cocktail (PIC) I (Sigma-Aldrich), 1x PIC II (Sigma-Aldrich), 0.5% NP40 in 1x TBS) for 20 min, centrifuged for 10 min at 10 000 g at 4°C and supernatant was recovered. Subsequently, lysates were incubated with Streptactin Sepharose resin (IBA) for 2 h at 4°C on a rotation wheel. After incubation, lysates were transferred onto Micro Bio-Spin columns (0.8 ml, BioRad), washed 3 times with TAP-wash buffer (1x PIC I, 1x PIC II, 0.1% NP40 in 1x TBS) and incubated with TAP-elution buffer (50 µM Desthiobiotin (IBA) in 1x TBS) at 4°C for 10 min before elution by centrifugation at 100 g for 10 s. Eluates were incubated with anti-Flag M2 resin (Sigma-Aldrich) for 2 h at 4°C on a rotation wheel, washed once with TAP-wash buffer, twice with TBS, and eluted by incubating samples with Flag elution buffer (200 µg/ml Flag peptide (Sigma-Aldrich) in 1x TBS) for 10 min following centrifugation for 10 s at 2000 g. TAPs were performed in triplicates from cells harvested on different days.

## 2.11 | Processing of TAP proteins for mass spectrometry and analysis

Eluates were reduced with 10 mM Dithiothreitol (DTT) for 30 min at 56°C, followed by alkylation with 55 mM Chloroacetamide (CAA) for 30 min at RT in the dark. Subsequently, samples were boiled in Laemmli buffer (1x final concentration 2% SDS, 2 µM DTT, 5% (v/v) Glycerol, 50 µM Tris-HCL (pH 6.8, 0.01% (w/v) Bromophenol blue)) at 95°C for 10 min and run for approx. 1 cm in a 10% SDS-PAGE gel to separate purified proteins from the Flag peptide used for elution. Gels were fixed in fixation buffer (45% H<sub>2</sub>O, 45% MeOH, 10% Acetic acid) for 1 h at RT and stained (fixation buffer, 0.05% Coomassie-G250, filtered) for 1 h at RT followed by a first destaining in fixation buffer for

1 h before destaining O/N. Protein lanes were separated, cut into small pieces, washed twice with MS-wash buffer (50 mM Ammonium bicarbonate (ABC), 50% Acetonitrile (ACN)) for 20 min, dehydrated with ACN for 10 min, and dried in a speed vac for 20 min. Afterward, samples were washed with 50 mM ABC for 15 min at RT, and dehydration was repeated with speed vacuuming for 30 min. For in-gel-digest of proteins, gel pieces were soaked in digest solution (0.009 µg/µl Trypsin, 0.001 µg/µl LysC, 45 mM ABC) for 30 min at 4°C, covered with 50 mM ABC and digested O/N at 37°C. Supernatants were recovered, gel pieces incubated in extraction buffer (30% ACN, 3% Trifluoroacetic acid (TFA)) for 20 min at RT, supernatants were recovered, and proteins were extracted from gel pieces by incubation in 100% ACN for 20 min at RT with recovery of supernatants. The recovered supernatants of individual samples were pooled, organic solvents were evaporated in a speed vac, samples were acidified with Formic acid (1% final concentration), stage tipped, and subjected to mass spectrometry.

## 2.12 | TAP mass spectrometry

Raw mass spectrometry data files were analyzed using MaxQuant software (version 1.6.0.16). Further analysis of quantitated proteins was done with Perseus software (version 1.5.5.3). Data were cleaned by filtering out reverse proteins, proteins only identified by site and contaminants, and filtered for valid proteins label-free quantification (LFQ) values identified in at least two technical replicates in at least one condition. Further analysis of data was done using R software. Missing LFQ values were imputed using the DEP package (version 1.6.1) by firstly imputing of missing not at random (MNAR) values with 0, followed by a screen for falsely categorized MNAR values and re-imputation of missing at random (MAR) values using the *k*-nearest neighbors (knn) algorithm. For statistical analysis of differentially enriched (DE) proteins, a two-tailed *t*-test with unequal variance was applied to conditions containing Crel2 protein versus the respective mock control (acute or stable). Proteins with fold change > 0 (Crel2 containing conditions versus mock control) and *p*-value < .1 were considered DE.

## 2.13 | Patients and ethics

The study protocol conformed to the revised Declaration of Helsinki (Edinburgh, 2000) and was approved by the local Institutional Review Board (Ethik-Kommission am

Universitätsklinikum Essen; file number 09-4252). All patients provided written informed consent for participation in the study before recruitment. Liver tissue and serum were collected from morbidly obese patients undergoing bariatric surgery. All enrolled patients underwent physical and ultrasound examinations and a complete set of laboratory studies. Subjects reporting excessive alcohol consumption (>20 g/day for men or >10 g/day for women) and those with other known causes of secondary fatty liver disease (e.g., viral hepatitis, metabolic liver disease, toxic liver disease) were excluded from the study. Histological evaluation of NAFLD and classification as NAFL or NASH were performed by two experienced pathologists according to the method of Bedossa et al (SAF score<sup>38</sup>).

## 2.14 | CRELD2 ELISA

Serum CRELD2 levels were measured using a human CRELD2 Elisa kit (Ray Biotech) according to the manufacturers' instructions.

## 2.15 | Immunoblotting

### 2.15.1 | Human tissue samples

Liver tissue was directly lysed for 30 min on ice with RIPA Lysis and Extraction Buffer (Thermo Scientific) containing protease inhibitor cocktail and phosphostop (Roche). After centrifugation at 13 000 g for 15 min at 4°C, protein concentration in the supernatant was measured using Bradford's reagent (Bio-Rad).

### 2.15.2 | Mouse tissue samples

Tissue was snap-frozen in liquid N<sub>2</sub> and stored at −80°C until usage. Tissue was homogenized in RIPA buffer containing PIC I and PIC II (Sigma-Aldrich) and Complete protease inhibitor (Roche) using a Precellys homogenizer and lysed for 30 min on ice. 10–20 µg of total protein were separated by SDS-PAGE and transferred onto a PVDF membrane (Immobilon-P transfer membranes 0.45 µm, Merck) via semi-dry blotting (Trans-Blot Turbo Transfer System, Bio-Rad). If not otherwise mentioned, membranes were incubated with antibodies diluted in TBST (0.1% Tween20) overnight at 4°C on a rocker with the particular antibodies (see Table S3). Protein band intensities were acquired using ImageJ2. Proteins of one membrane were normalized to Actin and set relative to a wildtype control located on the membrane.

## 2.16 | Statistical analysis and reproducibility

Data are shown as mean, with individual values per mouse represented as circles, unless stated otherwise. Statistical significance was analyzed with R using unpaired two-tailed *t*-tests, one-way and two-way ANOVA as indicated in the figure legends. The *n* value represents biological replicates. Significance was considered at *p* < .05. Experiments were repeated to ensure the reproducibility of the observations. No statistical methods were used to predetermine sample size.

## 3 | RESULTS

To investigate *Creld2* function in vivo, we generated a *Creld2*-knockout mouse model by replacing the endogenous locus with an enhanced green fluorescent protein (eGFP) (*Creld2*<sup>eGFP/eGFP</sup>, Figure 1A), allowing the use of both *Creld2*<sup>WT/eGFP</sup> and *Creld2*<sup>eGFP/eGFP</sup> as reporter mice for *Creld2* expression. We confirmed ubiquitous protein expression<sup>39</sup> and lack of *Creld2* expression in *Creld2*<sup>eGFP/eGFP</sup> mice in various tissues via immunoblotting (Figure 1B). *Creld2*<sup>eGFP/eGFP</sup> mice were born in Mendelian ratios (Figure 1C) and were viable. In concordance with studies of *Atf6*<sup>−/−</sup> mice, which do not show any abnormal phenotype during steady-state,<sup>21</sup> young *Creld2*<sup>eGFP/eGFP</sup> mice (1–2 month-old) did not show differences in body and liver weight (Figure 1D,E) or changes in tissue morphology as assessed histologically via hematoxylin-eosin (HE) and Masson-Goldner Trichrome (MGT) stain (Figure 1F).

Given that *Atf6* induces *Creld2* expression and that *Atf6* was shown to regulate responses under high-fat diet-induced obesity,<sup>28</sup> we asked whether *Creld2* is involved in regulating metabolic responses due to prolonged accumulation of lipids in hepatocytes. To induce the development of fatty liver, we placed 8-week-old *Creld2*<sup>eGFP/eGFP</sup> males and wildtype littermates on a control diet (CD) or high-fat diet (HFD). To test whether animals could recover from hepatosteatosis, we split the HFD group after eight weeks: one group remained on HFD for four more weeks, and one group was switched to CD (HFD > CD, Figure 2A). Measuring mice body weights, we found that *Creld2*<sup>eGFP/eGFP</sup> animals on CD gained less weight over time (Figure 2B). Similarly, after 8–12 weeks on HFD *Creld2*<sup>eGFP/eGFP</sup> showed reduced body weights compared to littermate controls (Figure 2B) but developed insulin resistance as measured by the homeostatic model assessment indices of insulin resistance (HOMA-IR) after eight weeks (Figure 2C). Moreover, both genotypes increased the total tissue weight of livers and epididymal white adipose tissue



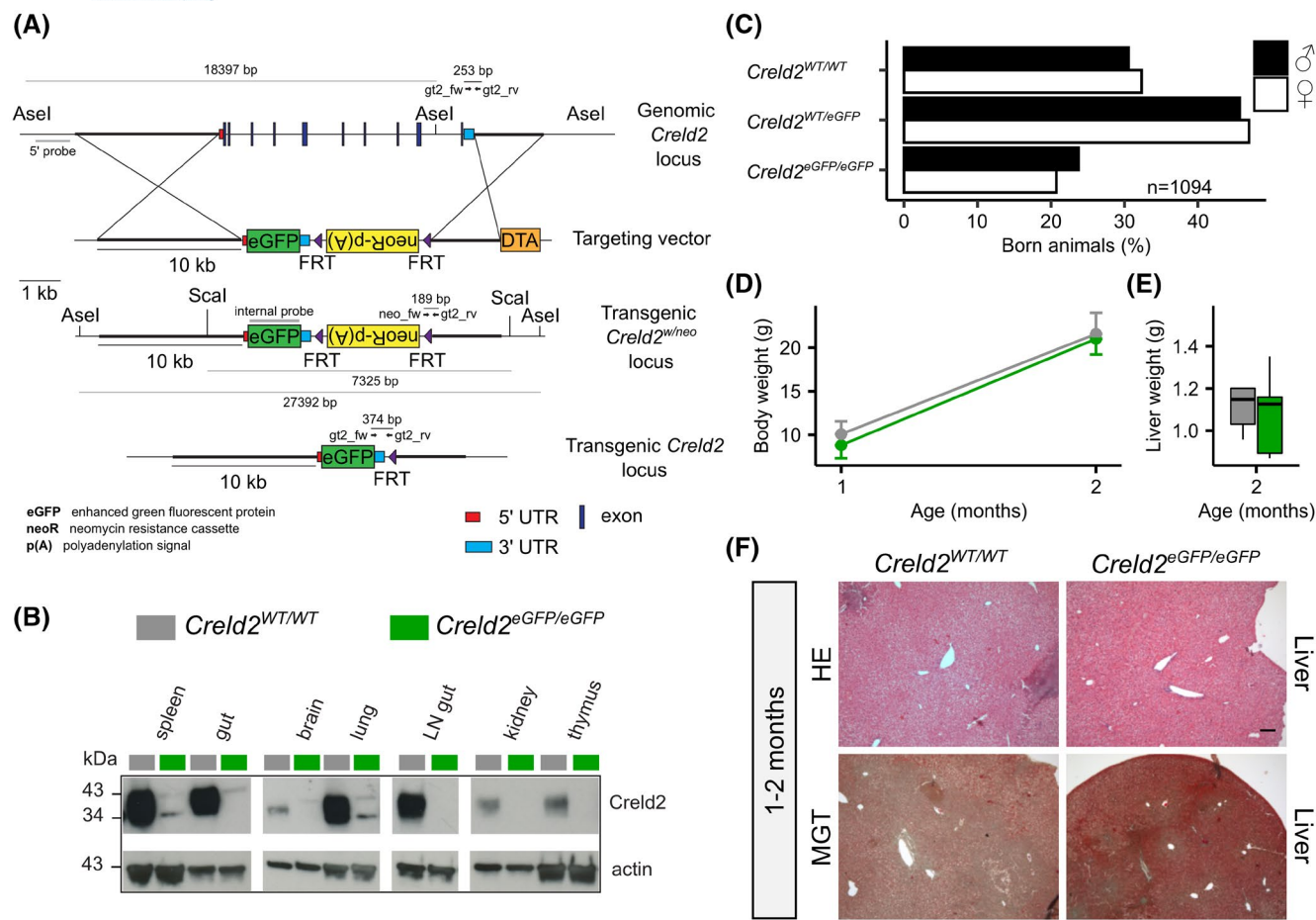


**FIGURE 1** Generation and phenotypic analysis of the *Creld2*<sup>eGFP/eGFP</sup> mouse. (A) Gene targeting strategy. The complete genetic locus of *Creld2* was replaced by an eGFP reporter via homologous recombination. The targeting vector comprised a neoR cassette flanked by FRT sites for positive ES cell selection. Following recombination, the neoR cassette was excised by FLP-mediated deletion. Primers for ES cell screening (gt2\_fw, gt2\_rv, neo\_fw) and probes used for Southern blotting (5' probe, internal probe) and the resulting fragment lengths (bp) are indicated. (B) Tissue expression profile of *Creld2* and testing of the anti-*Creld2* antibody specificity by immunoblotting. (C) Animals born from *Creld2*<sup>WT/GFP</sup> × *Creld2*<sup>WT/GFP</sup> matings. (D) Bodyweight of males (1 month: n = 5–7 and 2 months: n = 44–50). Error bars represent ± SD. (E) Liver weight of males (2 months: n = 5). Unpaired two-tailed t-test. (F) Histological analysis of liver by hematoxylin-eosin (HE) and Masson Goldner trichrome (MGT) in young *Creld2*<sup>eGFP/eGFP</sup> and wildtype mice. Representative for n = 8–10

(eWAT) (Figure S1A), indicating that *Creld2*<sup>eGFP/eGFP</sup> animals were not protected from diet-induced obesity.

Histological assessment of the liver showed an increased oil-red-O (ORO) staining in HFD-fed mice (Figure S1B,C), indicating increased neutral lipid storage. This was accompanied by a decrease in PAS signal (Figure S1D,E), confirming diet-induced hepatosteatosis in both genotypes. Accumulation of lipids in general, which resulted mainly from TAG and DAG accumulation, was confirmed by shotgun lipidomics (Figure 2D). *Creld2*<sup>eGFP/eGFP</sup> livers generally contained fewer lipids (Figure 2D), which could account for the lower liver weight (Figure S1A). HFD did not induce a fibrotic phenotype, nor did it affect liver function as assessed by MGT staining (Figure S1F,G) and alanine aminotransferase (ALT) concentrations in the serum (Figure S1H), respectively. When the HFD groups were switched to CD, their body, liver, and eWAT weight

returned to the level of animals kept on CD (Figures 2B and S1A). Further, ORO and PAS signals and the amount of lipids returned to baseline levels in both genotypes (Figures 2D and S1B–E). Together, our data indicate that *Creld2*-deficient mice responded similarly to wildtype mice on organismal and tissue level upon diet-induced obesity and lipid uptake as well as mobilization of lipids after a diet switch from HFD to CD.

To test whether lipid accumulation or subsequent lipid mobilization triggered differential cellular stress responses in *Creld2*<sup>eGFP/eGFP</sup> and littermate control livers, we performed RNA-sequencing (RNA-seq) after 12 weeks on diet (Figures 2E,F and S1I). We made use of Construction of Co-expression network analysis 2 (CoCena<sup>2</sup>) to cluster the top 5000 variable genes into distinct modules based on the expression patterns across the two genotypes and three conditions (Figure 2E).



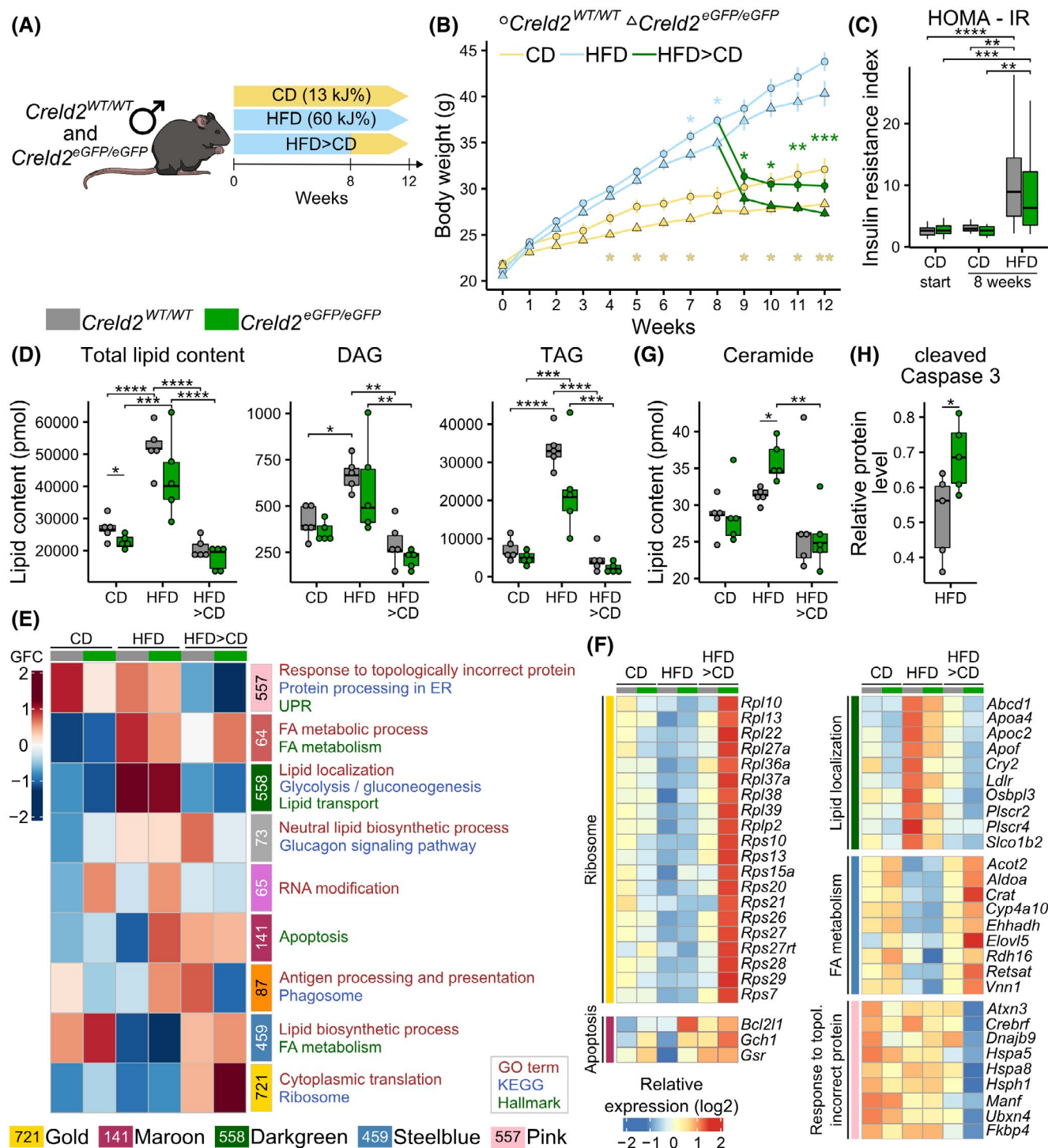


**FIGURE 2** Tissue and molecular response of *Creld2*<sup>eGFP/eGFP</sup> mice to a high-fat diet. (A) Experimental setup. (B) Bodyweight of male mice fed with CD (control diet; n = 13–14) and HFD (high-fat diet; n = 12–31) for 12 weeks, or HFD for 8 weeks following CD for 4 weeks (n = 14–19). (C) Analysis of insulin resistance induction by HFD via HOMA-IR (homeostatic model assessment of insulin resistance, CD start: n = 22–29; CD 8 weeks: n = 7–10; HFD 8 weeks: n = 17–20). One-way ANOVA with Tukey post-hoc test. (D) Lipid mass spectrometry of livers (n = 5 per condition). DAG: Diacylglycerol. TAG: Triacylglycerol. Circles represent individual mice. One-way ANOVA. (E) Co-expression network analysis (CoCena) performed on RNA-seq data of livers (n = 5 per condition). Numbers indicate genes belonging to a module. Colors represent cluster names: pink: 557 genes, Indian red: 64 genes, dark green: 558 genes, dark gray: 73 genes, orchid: 65 genes, maroon: 141 genes, dark orange: 87 genes, steel blue: 459 genes, gold: 721 genes. GFC: group fold change. (F) Heatmap representation of selected genes from (E), values are displayed as z scores. (G) Lipid mass spectrometry analysis for ceramides. Circles represent individual mice. One-way ANOVA with Tukey post-hoc test. (H) Western blot analysis for cleaved Caspase 3 (n = 5). Circles represent individual mice. Unpaired two-tailed t-test. \**p* < .05, \*\**p* < .01, \*\*\**p* < .001, \*\*\*\**p* < .0001

CoCena identified the gold module (721 genes) with globally upregulated genes in *Creld2<sup>eGFP/eGFP</sup>* livers showing the highest differences after HFD > CD diet (Figure 2E). Gene Ontology (GO) and KEGG enrichment analyses indicated enrichment for cytoplasmic translation as well as ribosome proteins and ribosome production (Figure 2F). Additionally, the maroon module showed induction of 141 genes in *Creld2<sup>eGFP/eGFP</sup>* livers after HFD. This module contained ‘apoptosis’ as Hallmark term (Figure 2E), including the genes *Bcl2l1*, *Gch1*, and *Gsr* (Figure 2F), suggesting that knockout livers may experience more apoptosis than wildtype controls. This notion was supported by increased ceramide levels in *Creld2<sup>eGFP/eGFP</sup>* livers after HFD (Figure 2G), as their accumulation has been associated with apoptosis in hepatosteatosis.<sup>40</sup> Indeed, immunoblotting against cleaved Caspase3 confirmed that *Creld2<sup>eGFP/eGFP</sup>* livers after HFD underwent increased apoptosis compared to *Creld2<sup>WT/WT</sup>* (Figures 2H and S1J).

Further, CoCena identified the darkgreen module, which contains highly expressed genes after HFD that are globally downregulated in *Creld2<sup>eGFP/eGFP</sup>* livers compared to *Creld2<sup>WT/WT</sup>* in each condition (Figure 2E and Table S4). GO and Hallmark terms indicated that many of the 558 genes were involved in regulating lipid localization and transport. Among these genes, we found apolipoprotein genes (*Apoa4*, *Apoc2*, *Apof*), which are important for lipid transport, genes involved in lipid distribution (*Abcd1*, *Ldlr*, *Osbp13*, *Plscr2/4*, *Slco1b2*), and the circadian rhythm regulating transcription factor *Cry2*, which is responsible for the orchestration of physiological metabolism (Figure 2F).

The steelblue module (459 genes) includes genes upregulated in *Creld2<sup>eGFP/eGFP</sup>* animals during CD and HFD > CD recovery diets. Many of these genes are associated with fatty acid (FA) metabolism, mostly involving genes for lipid catabolism (*Acot2*, *Ehhadh*, *Cyp4a10*, *Rdh16*) and some genes responsible for lipid anabolic processes (*Aldoa*, *Elovl5*) (Figure 2F), which might explain why *Creld2<sup>eGFP/eGFP</sup>* animals and livers show reduced lipid amounts as they upregulate these genes even more than *Creld2<sup>WT/WT</sup>* after HFD > CD recovery.

The pink module returned 557 genes downregulated in *Creld2<sup>eGFP/eGFP</sup>* livers compared to controls, particularly in the HFD > CD condition. These genes were involved in “responses to topologically incorrect protein,” “protein processing in the ER,” and the ‘UPR’ based on GO, KEGG, and Hallmark enrichment analyses. Among these genes were chaperones and co-chaperones (*Dnajb9*, *Hspa8*, *Hsph1*, *Fkbp4*), including *Hspa5* (*Grp78*) (Figure 2F). Therefore, we investigated whether *Grp78* expression and UPR activation were affected on a protein level. However, neither *Grp78* nor phosphorylation levels of *Perk* and

*eIF2 $\alpha$*  were significantly changed in *Creld2<sup>eGFP/eGFP</sup>* livers compared to littermate controls (Figure S1J,K). Further, the comparison of CD versus HFD groups per genotype did not reveal any sign of induced ER stress on transcript or protein level (Figures 2F and S1J,K), with *Grp78* and *Chop* expression being even downregulated after HFD when compared to CD (Figure S1J,K). To test for other targets of the UPR that might be affected by the dietary change and that were possibly not included in the CoCena<sup>2</sup> analysis, we additionally performed a direct pairwise comparison of differentially expressed genes ( $\text{lfc} = 1.32$ ;  $p\text{-value} = .05$ ) between CD or HFD in *Creld2<sup>WT/WT</sup>* or *Creld2<sup>eGFP/eGFP</sup>* animals. None of these analyses returned genes involved in UPR (Table S5), indicating that 12 weeks of HFD do not induce ER stress in the liver.

Taken together, our data suggest that *Creld2<sup>eGFP/eGFP</sup>* animals can generally cope with an excess of lipid uptake for a short period of 12 weeks, despite transcriptional changes that hint toward altered lipid metabolic processes. Furthermore, neither transcriptome nor protein expression analysis revealed a lipid-driven ER stress response in the liver, despite an enhanced apoptotic phenotype in *Creld2<sup>eGFP/eGFP</sup>* mice livers.

Next, we turned to the question of whether *Creld2* is involved in the resolution of ER stress. To this end, *Creld2<sup>eGFP/eGFP</sup>* animals and littermate controls received a single intraperitoneal injection of the ER stressor Tm (1 mg/kg) or sucrose as a control since Tm was prepared in a sucrose solution (Figure 3A). Two days post-injection, mice were analyzed for the extent of fatty liver development, which served as a surrogate readout of unresolved ER stress (Figure 3B,C). Histological analyses and shotgun lipidomics indicated that *Creld2<sup>WT/WT</sup>* livers did not accumulate significant amounts of lipids or glycogen after Tm injection, while an increase of lipids after Tm injection was observed in *Creld2<sup>eGFP/eGFP</sup>* livers (Figures 3B,C and S2A,B). The slightly increased lipid storage in *Creld2<sup>WT/WT</sup>* animals primarily resulted from the accumulation of cholesterol and cholesterol esters (Figure 3C). However, *Creld2<sup>eGFP/eGFP</sup>* livers stored significantly more lipids than *Creld2<sup>WT/WT</sup>* controls after Tm treatment, mainly attributed to augmented TAG, DAG, and cholesterol ester abundance (Figure 3B,C). This fatty liver phenotype was accompanied by a decreased PAS signal (Figures 3B and S2C). Furthermore, MGT revealed an increased collagen abundance after Tm treatment in both genotypes (Figure S2D,E).

To identify the molecular mechanisms that led to the augmented lipid accumulation in *Creld2<sup>eGFP/eGFP</sup>* mice after ER-stress induction with Tm, we performed RNA-seq on livers and analyzed the gene expression using principal component analysis (PCA, Figure S2F) and CoCena<sup>2</sup> (Figure 3D and Table S6). The maroon module (1308

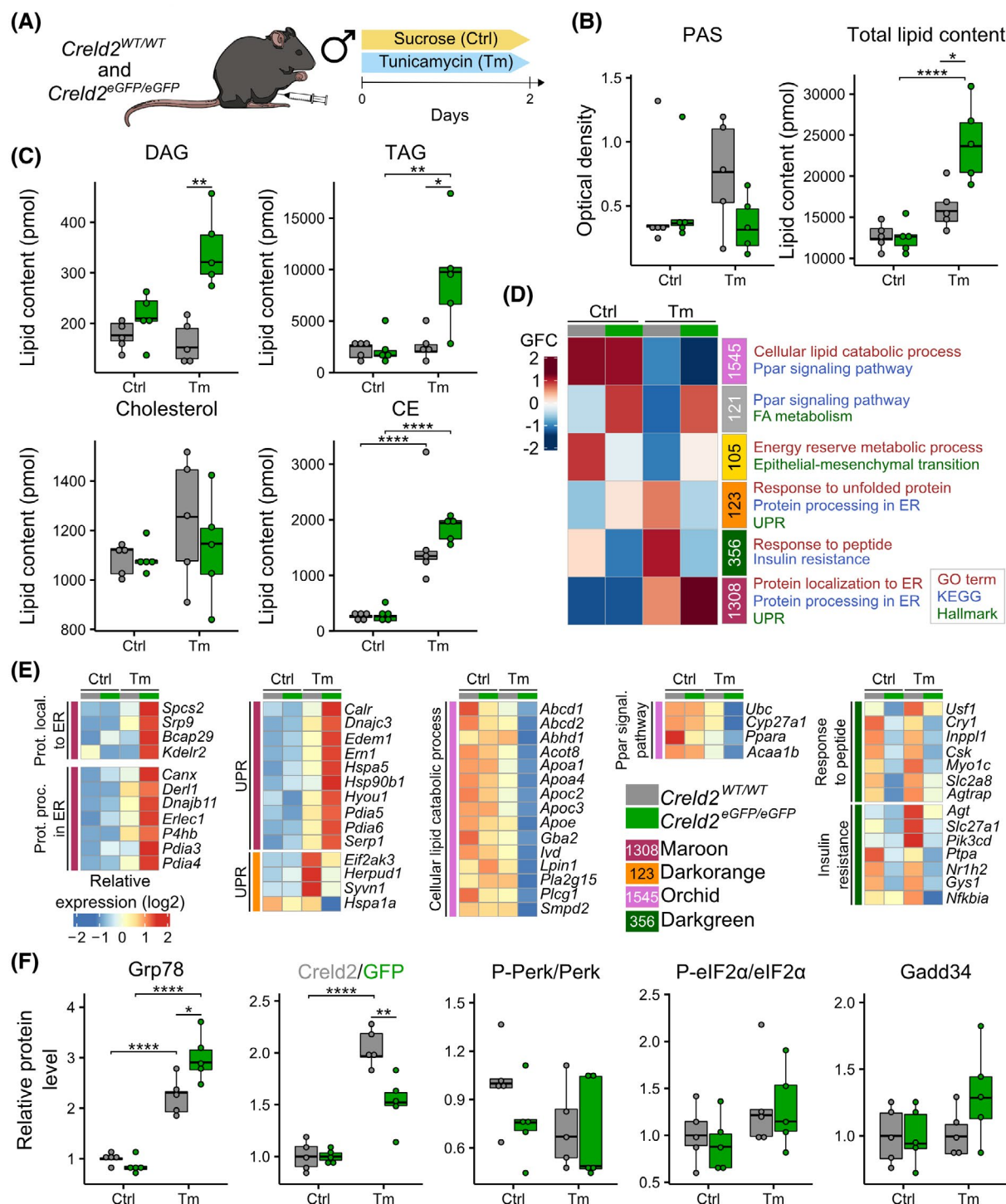


**FIGURE 3** Tissue and molecular response of *Creld2*<sup>eGFP/eGFP</sup> mice to pharmacological ER stress induction. (A) Experimental setup. (B) Quantification of liver PAS stainings and mass spectrometrical assessment of liver lipids ( $n = 5$  per condition). Circles represent individual mice. One-way ANOVA with Tukey post-hoc test. (C) Lipid mass spectrometry of livers ( $n = 5$  per condition). DAG: Diacylglycerol. TAG: Triacylglycerol. CE: Cholesteryl esters. Circles represent individual mice. One-way ANOVA with Tukey post-hoc test. (D) Co-expression network analysis (CoCena) performed on RNA-seq data of livers ( $n = 5$  per condition). Numbers indicate genes belonging to a module. Colors represent cluster names: orchid: 1545 genes, dark grey: 121 genes, gold: 105 genes, dark orange: 123 genes, dark green: 356 genes, maroon: 1308 genes. GFC: group fold change. (E) Heatmap representation of selected genes from (D), values are displayed as z scores. (F) Western blot analysis for UPR components ( $n = 5$  per condition). For Perk and eIF2 $\alpha$ , ratios of phosphorylated (P-Perk and P-eIF2 $\alpha$ ) and unphosphorylated protein abundance are displayed. Circles represent individual mice. One-way ANOVA with Tukey post-hoc test. \*  $p < .05$ , \*\*  $p < .01$ , \*\*\*  $p < .001$ , \*\*\*\*  $p < .0001$ .



genes) contains genes upregulated after Tm treatment in both genotypes compared to untreated mice, with even a higher expression in *Creld2*<sup>eGFP/eGFP</sup> livers. GO, KEGG, and Hallmark enrichment analyses returned terms such as “protein localization to ER,” “protein processing in ER” and “UPR” (Figure 3D), which comprised UPR- (*Hspa5*, *Hsp90b1*, *Ern1*) and ERAD-related genes (*Derl1*, *Edem1*, *Pdia3*, *Pdia4*, *Erlec1*) (Figure 3E). Tm treatment prevents protein glycosylation, inducing ER stress and lipid accumulation<sup>20</sup> (Figure 3B,C). Wildtype livers largely recover from Tm-induced lipid perturbations after 2–3 days while keeping part of the UPR active, for example, expression of chaperones Grp78 and Grp94 (*Hsp90b1*).<sup>20,27</sup> Our data validate these observations showing that UPR is active after two days of Tm treatment. Furthermore, this suggests that *Creld2*<sup>eGFP/eGFP</sup> livers undergo elevated ER stress compared to *Creld2*<sup>WT/WT</sup> controls. In contrast, the darkorange module (123 genes) identified genes that are downregulated in *Creld2*<sup>eGFP/eGFP</sup> livers and that also belong to the UPR (e.g., *Perk*/*Eif2ak3*) (Figure 3D,E). These two CoCena<sup>2</sup> modules suggest that *Creld2*<sup>eGFP/eGFP</sup> mice are only partly inducing the UPR under ER stress and, therefore, are incapable of resolving ongoing ER stress correctly. This, in turn, results in increased hepatic lipid storage, supporting the active role of *Creld2* during UPR and subsequent ER protein processing capacity upon acute ER-stress challenge.

In line with this hypothesis, the module orchid (1545 genes) classified genes downregulated after Tm treatment in both genotypes, with even stronger downregulation in *Creld2*<sup>eGFP/eGFP</sup> livers (Figure 3D). GO and KEGG enrichment analysis of genes in the orchid module included mainly terms related to “cellular lipid catabolic process” and “Ppar signaling pathway” (Figure 3D). This might explain why *Creld2*-deficient livers store an increased amount of lipids since genes essential for lipid catabolism (*Abcd1*, *Abcd2*, *Abhd1*, *Acot8*, *Gba2*, *Ivd*, *Pla2g15*, *Plcg1*, *Ppara*, *Acaa1b*) and lipid transport (*Apoa1*, *Apoa4*, *Apoc2*, *Apoc3*, *Apoe*) were downregulated (Figure 3E).

The module dark green identified 356 genes globally downregulated in *Creld2*<sup>eGFP/eGFP</sup> livers, with the highest differences after Tm treatment (Figure 3D). These genes enriched largely for “response to peptide” and “insulin resistance” as determined by GO and KEGG pathway enrichment analyses. Among enzymes regulating energy homeostasis were *Slc27a1*, *Gys1*, and *Nr1h2* (insulin resistance), as well as *Usp1*, *Cry1*, and *Slc2a8* (response to peptide), which collectively regulate lipid and glucose metabolism. In addition, expression of genes associated with signal transduction (*Pik3cd*, *Nfkb1a*) and regulation of cellular growth (*Ptpa*, *Inpp1l1*, *Csk*) was disrupted in *Creld2*<sup>eGFP/eGFP</sup> livers, exhibiting further aspects of *Creld2*-dependent regulatory processes (Figure 3E). Summarized, CoCena<sup>2</sup> analyses of Tm challenged livers reveal a

*Creld2*-dependent dysregulation of genes important for the resolution of ER stress resulting in altered lipid and glucose metabolism and cellular signaling processes in *Creld2*-deficient mice livers, which subsequently leads to increased lipid storage.

To test this hypothesis, we first analyzed Grp78 protein abundance after Tm treatment as an indicator for protein accumulation in the ER lumen. Similar to RNA-seq results, Grp78 was upregulated in wildtype animals after Tm compared to control treatment but was even more abundant in *Creld2*<sup>eGFP/eGFP</sup> livers (Figures 3F and S2G). Of note, both GFP expression in *Creld2*<sup>eGFP/eGFP</sup> and *Creld2* expression in *Creld2*<sup>WT/WT</sup> littermate controls was increased upon both treatment conditions (Figures 3F and S2G), rendering *Creld2* expression and the *Creld2*<sup>WT/eGFP</sup> mouse model as an efficient tool to monitor cellular stress. We next tested the activation of the Perk-axis via analysis of Perk and eIF2α phosphorylation and Gadd34 protein abundance. Despite increased levels of Grp78, we did not detect enhanced activation of the Perk axis in *Creld2*<sup>eGFP/eGFP</sup> livers (Figures 3F and S2G). In summary, induction of ER stress via Tm causes exacerbated ER stress in *Creld2*<sup>eGFP/eGFP</sup> mice, as indicated by increased Grp78 expression and consequently augmented hepatic lipid storage, supporting the notion that *Creld2* is required to maintain tissue homeostasis in order to prevent lipid accumulation due to long-lasting and unresolved ER stress.

To investigate the molecular function of *Creld2* in UPR and metabolic homeostasis, we performed co-immunoprecipitation experiments by tandem affinity purification<sup>41</sup> and subsequent mass spectrometry. We used murine *Creld2* tagged either at the N- or C-terminus to exclude inhibition of protein binding due to the fused Strep-Flag tag. *Creld2* constructs were either transiently expressed (72 h) or stably integrated into the genome of HEK239 cells (Figure 4A) to (i) enable the characterization of specific interactions with chaperones, since a strong transient overexpression increases the unspecific co-purification of heat shock proteins<sup>41</sup> and (ii) select for highly conserved interactions, which would also occur in this inter-species (mouse-human) setup. Using a stringent filtering pipeline and imputation for missing values (Figure 4B, see also methods), we found 31 putative interaction partners (Figure 4C and Table S7). Analysis for GO enrichment returned terms such as ‘response to ER stress’, ‘protein folding’, and ‘cell redox homeostasis’ (Figure 4D). Many chaperones and PDI were present in the transient condition (C2-SF trans), some of which (HSPA8, HSP90B, HYOU1) have been previously proposed to interact with *Creld2*.<sup>7</sup> However, since these proteins were not enriched in the stably transfected cells (FS-C2 stab and C2-SF stab), we propose that these represent unspecific co-purification products,<sup>41</sup> underlining the constraints of



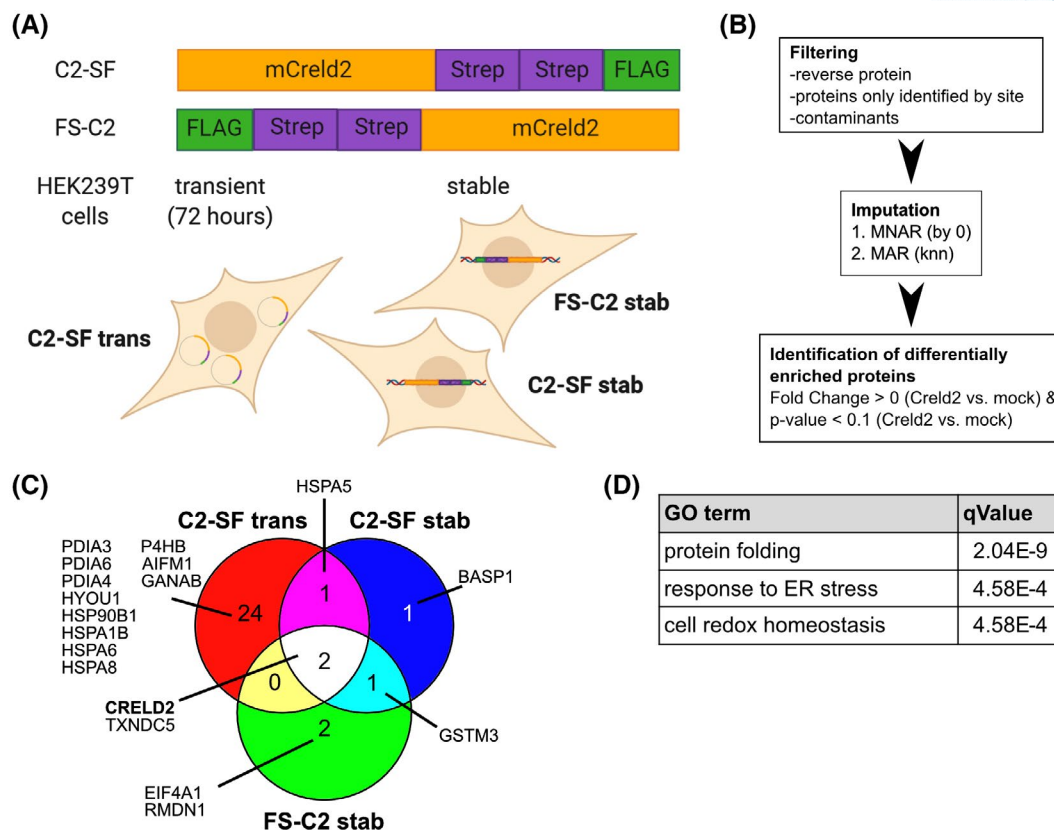


**FIGURE 4** Creld2 interacts with proteins involved in protein folding, response to ER stress, and detoxification. (A) Schematic representation of constructs and expression conditions used for tandem-affinity-purification of tagged murine Creld2. (B) Workflow chart for analysis of mass spectrometry data. MNAR values in the dataset were first imputed by 0, followed MAR imputation by knn algorithm. MNAR: missing not at random; MAR: missing at random; knn: *k*-nearest neighbors. (C) Enriched Creld2 interaction partners across the different expression conditions. (D) Top three enriched GO terms resulting from enrichment analysis of all co-purified proteins

co-immunoprecipitation assays in transiently transfected cell lines.

Thus, we focused our analysis on candidates present in at least two conditions. This identified Creld2, as expected, as well as HSPA5 (GRP78), thioredoxin domain-containing 5 (TXNDC5), and glutathione S-transferase Mu3 (GSTM3) as potent specific Creld2 binding partners (Figure 4C). Interaction with GRP78<sup>7</sup> further endorses an active role of Creld2 in regulating UPR, as it may sequester the chaperone away from Perk/Atf6/Ire1, thereby promoting the activation of the three UPR axes. TXNDC5, also known as endo PDI, is a thioredoxin peroxidase whose expression is regulated by ATF6 and sXBP1. Functionally it is proposed to reduce misfolded protein load.<sup>42</sup> Intriguingly, also Creld2 has been proposed to have PDI-like functions,<sup>7</sup> hinting towards a synergistic mechanism between these proteins to resolve ER stress. GSTM3 is a member of the glutathione S-transferases superfamily that promotes the detoxification of reactive oxygen species (ROS).<sup>43</sup> Oxidative stress and UPR are tightly interlinked, exemplified by PERK acting upstream of the transcription factor NRF2 that counteracts the toxic effects of ROS

produced upon ER stress during protein folding, e.g., via PDI activity.<sup>44</sup> Thus, the interaction of Creld2 with GSTM3 may represent an additional point of crosstalk between these cellular stresses. In summary, our data support the hypothesis of Creld2 being involved in the UPR, probably via the interaction with chaperones and enzymes whose activity is required to overcome cellular stress.

Overall, our data suggested that Creld2 function is required to maintain hepatic homeostasis under ER-stress responses in mice. Therefore, we next asked whether human CRELD2 would play a role under pathophysiological conditions in the liver and analyzed a cohort of 57 obese patients with varying severity of non-alcoholic fatty liver disease (NAFLD) and four controls for CRELD2 expression. We first divided patients into two groups—with or without non-alcoholic steatohepatitis (NASH) as diagnosed using the SAF (Steatosis, Activity, and Fibrosis) score, which increases with disease progression.<sup>38</sup> Intriguingly, both CRELD2 transcript and protein levels in the liver were significantly upregulated in male patients with NASH, while expression in female patients remained unaffected (Figure 5A).

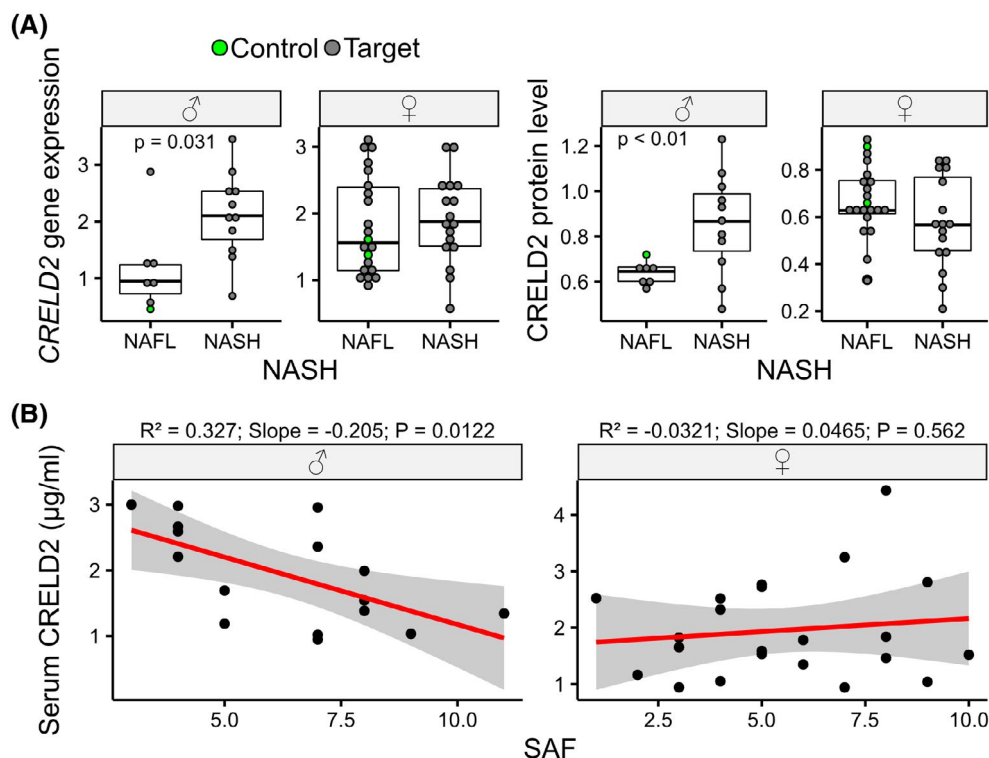


**FIGURE 5** Hepatic CRELD2 expression increases in patients with non-alcoholic steatohepatitis. (A) Hepatic gene and protein expression levels of CRELD2 in male (♂) and female (♀) non-alcoholic fatty liver disease (NAFLD) patients (gray circles) with or without NASH (non-alcoholic steatohepatitis) and healthy controls (green circles). The cohort is comprised of 57 patients. Circles represent individual patients. Unpaired two-tailed *t*-test. (B) Analysis of CRELD2 serum concentration in male (♂) and female (♀) patients plotted against the Steatosis Activity and Fibrosis (SAF) score (cohort comprised of 40 patients). Linear regression model. Circles represent individual patients

Control patients showed similar expression to NAFL patients. To test whether secreted CRELD2 could be used as a diagnostic marker for NAFLD severity, we plotted the serum concentration of CRELD2 against the SAF score (Figure 5B). While no correlation was observed in female patients, males showed an inverse correlation with low levels of CRELD2 at higher SAF scores, which may hint towards a retention mechanism for CRELD2 in the tissue during hepatic pathophysiology. In summary, CRELD2 shows a sex-specific function during NAFLD in humans with an intra-hepatic upregulation of CRELD2 expression, which seems to be associated with progression to NASH in male patients.

To address whether this sexual dimorphism can also be detected in mice, we analyzed ~1-year-old mice (12–15 months) since aging is correlated with the development of NAFLD,<sup>45,46</sup> and females do not correspond similarly to ER-stress induction via Tm treatment and HFD-induced obesity as males.<sup>47–49</sup> Thin-layer chromatography analyses revealed that male *Creld2*<sup>eGFP/eGFP</sup> livers accumulate more free fatty acids (FFA), DAG, cholesterol, and cholesteryl esters when compared to littermate controls, whereas TAG remain at similar levels as in *Creld2*<sup>WT/WT</sup> livers

(Figure 6A). Intriguingly, we noticed that *Creld2*<sup>eGFP/eGFP</sup> females were protected from developing a hepatosteatosis phenotype (Figure 6A). Histological analyses confirmed the increased lipid accumulation in male mice, with *Creld2*<sup>eGFP/eGFP</sup> animals presenting dilated sinusoids, abundant vacuoles in hepatocytes, and an increased signal after ORO staining (Figure 6B).

To investigate the underlying molecular mechanisms leading to lipid accumulation in *Creld2*<sup>eGFP/eGFP</sup> livers, we performed qRT-PCR analyses on key mediators of lipid homeostasis. We observed that genes encoding the transcription factor *Pgc1α* (*Ppargc1a*), components of fatty acid oxidation (*Acox1*), acylglycerol metabolism (*Apoc2*, *Dgat1*, *Dgat2*), and cholesterol storage (*Apob100*, *Lsr*) were downregulated in livers of *Creld2*<sup>eGFP/eGFP</sup> males compared to controls (Figure 6C and Table S8).

We next assessed whether *Creld2*<sup>eGFP/eGFP</sup> livers experience increased ER stress due to the accumulation of lipids by analyzing the expression of chaperones *Grp78* (*Hspa5*), *Grp94* (*Hsp90b1*), and the apoptosis inducer *Chop* (*Ddit3*). All three markers showed increased expression on a transcriptional level, indicating ongoing UPR (Figure 6C and

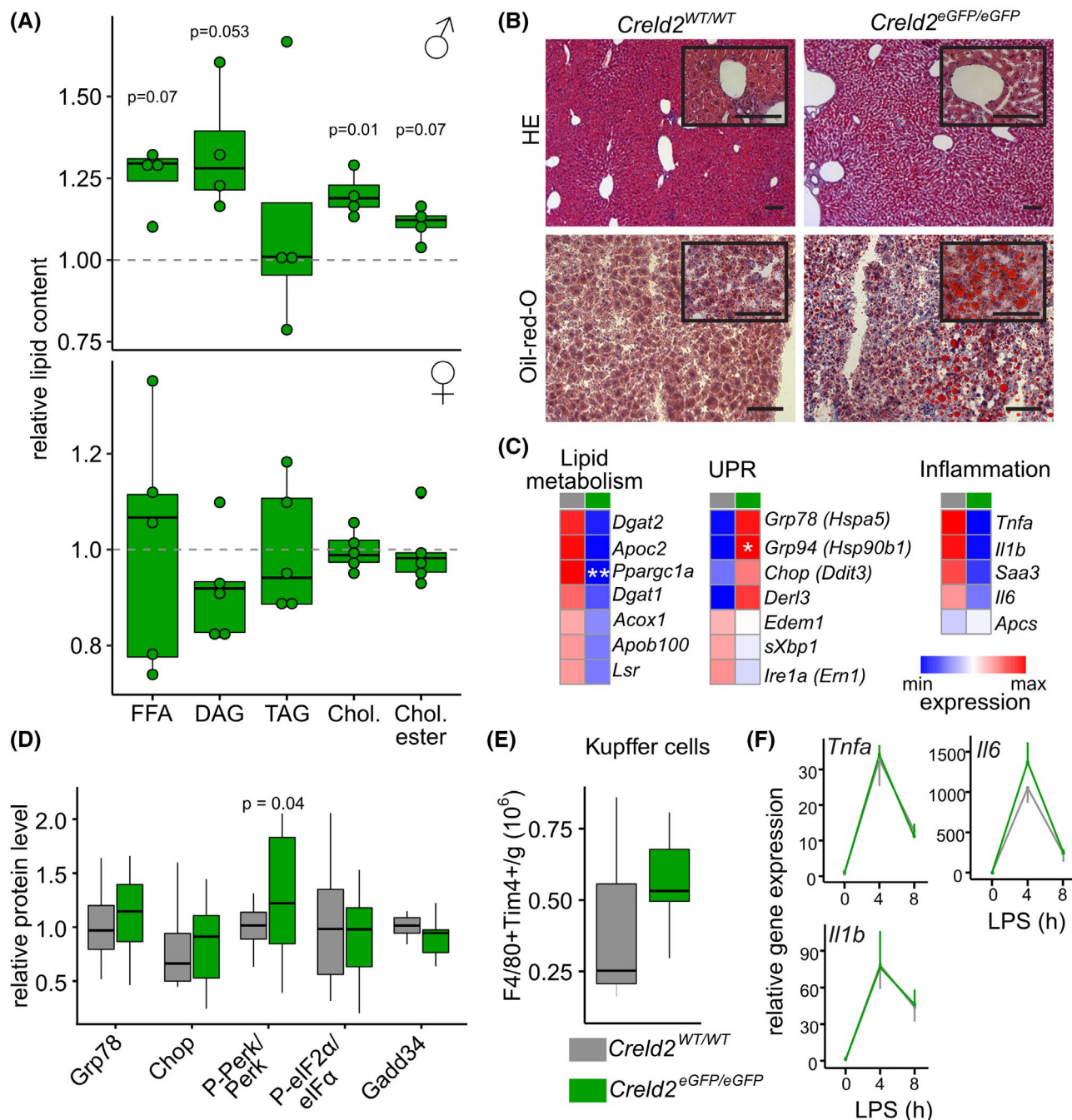


**FIGURE 6** *Creld2*<sup>eGFP/eGFP</sup> males develop liver steatosis with progressing age. (A) Thin-layer chromatography of total lipid extracts from 1-year-old animals (♂;  $n = 4$ , ♀;  $n = 3-5$ ). Circles represent individual mice; gray lines are means of control littermates. Unpaired two-tailed  $t$ -test. (B) Histological analysis of 1-year-old male livers by hematoxylin and eosin (HE) and Oil-red-O. Scale bars overview: 100  $\mu\text{m}$ . Scale bars insets: 10  $\mu\text{m}$ . (C) qRT-PCR analysis of male livers ( $n = 3-5$ ). Gene expression is displayed as relative value. Unpaired two-tailed  $t$ -test. \* $p < .05$ , \*\* $p < .01$ . (D) Protein expression in livers of male mice as assessed by western blot quantification ( $n = 17-19$ ). For Perk and eIF2 $\alpha$  ratios of phosphorylated (P-Perk and P-eIF2 $\alpha$ ) and unphosphorylated protein abundance are displayed. Unpaired two-tailed  $t$ -test. (E) Flow cytometry analysis of liver Kupffer cells (CD45<sup>+</sup>CD11b<sup>low</sup>F4/80<sup>+</sup>Tim4<sup>+</sup>) in male mice ( $n = 3-9$ ). (F) qRT-PCR analysis of pro-inflammatory cytokines *Tnfa*, *Il1b*, and *Il6* in bone-marrow-derived macrophages after LPS treatment isolated from males ( $n = 3-4$ ). Error bars represent  $\pm$  SD

Table S8). Albeit not significant, *Creld2*<sup>eGFP/eGFP</sup> livers also presented with higher Grp78 and Chop protein levels when compared to littermate controls (Figure 6C,D). Thus, we analyzed whether these changes activated the

three UPR axes, Atf6, Ire1, and Perk. Neither *Edem1* and *Derl3* as part of the ERAD machinery and downstream targets of Atf6<sup>13</sup> nor *Ire1* (*Ern1*) and *sXbp1* as part of the Ire1 pathway showed significant differences in gene



expression in male *Crelld2*<sup>eGFP/eGFP</sup> mice compared to controls (Figure 6C). Activation of the Perk pathway was determined through the phosphorylation status of Perk and eIF2 and the protein expression of Gadd34. We observed increased phosphorylation of PERK, suggesting that *Crelld2*<sup>eGFP/eGFP</sup> livers experience a low-grade ER stress; however, the signaling downstream of PERK was not altered compared to controls (Figure 6D). In line with the lack of hepatosteatosis, livers of female *Crelld2*<sup>eGFP/eGFP</sup> mice did not show significant transcriptional alterations in UPR or lipid metabolism pathways (Figure S3 and Table S8).

Next, we addressed whether increasing levels of inflammation and tissue damage, which are the basis for the progression of NAFLD to NASH, could be the leading cause of the dysregulated metabolism in aged *Crelld2*<sup>eGFP/eGFP</sup> males. qRT-PCR of pro-inflammatory cytokines (*Il1b*, *Il6*, *Tnfa*) and acute phase response genes (*Apcs*, *Saa3*) revealed an overall downregulation of these genes in *Crelld2*<sup>eGFP/eGFP</sup> livers compared to *Crelld2*<sup>WT/WT</sup> (Figure 6C and Table S8). Under steady-state, tissue-resident macrophages, also called Kupffer cells, are the main cytokine-producing cells in the liver. However, a comparison of their numbers revealed that *Crelld2*<sup>eGFP/eGFP</sup> livers harbor slightly more Kupffer cells (Figure 6E), suggesting that the reduction of cytokine expression was not due to reduced Kupffer cell numbers.

If the liver becomes inflammatory upon progression to NASH or fibrosis, monocytes are recruited to the liver, where they differentiate into macrophages and become a source of pro-inflammatory cytokines.<sup>50</sup> To test whether *Crelld2* deficiency could affect cytokine production of infiltrating macrophages, bone-marrow-derived macrophages (BMDMs) of 1-year-old male mice were treated with lipopolysaccharide (LPS), and the expression of *Tnfa*, *Il1b*, and *Il6* was assessed after 4 and 8 h of LPS treatment (Figure 6F). Both *Crelld2*<sup>eGFP/eGFP</sup> and *Crelld2*<sup>WT/WT</sup> controls showed peaking cytokine gene expression after 4 h, decreasing expression levels at 8 h of LPS stimulation, but no differences in transcript levels between both genotypes were observed (Figure 6F). Taken together, *Crelld2*-deficiency does not lead to severe UPR or directly affect the immunological response. Instead, our data suggest that lack of *Crelld2* function during steady-state results in a subthreshold ER stress and decreased expression of genes essential for lipid homeostasis, thereby evoking increased lipid storage in 1-year-old *Crelld2*<sup>eGFP/eGFP</sup> males.

## 4 | DISCUSSION

Our study shows that *Crelld2* contributes to the overall maintenance of cell homeostasis and the resolution of ER

stress (Figure 7). Using the newly generated *Crelld2*<sup>eGFP/eGFP</sup> transgenic mouse model, we characterized the hepatic stress response of *Crelld2*-deficient mice. *Crelld2*<sup>eGFP/eGFP</sup> mice do not show gross phenotypic differences during steady-state compared to wildtype controls at a young age. However, after a challenge with Tm, *Crelld2*-deficient livers show perturbed induction of UPR, which ultimately leads to dysregulated lipid homeostasis resulting in exacerbated development of NAFLD. These findings are congruent with previous reports about *Atf6* knockout mice,<sup>21,27</sup> suggesting the involvement of *Crelld2* in regulating a proper response to ER stress downstream of *Atf6*. This is further evidenced by the increased susceptibility of CRELD2-deficient Neuro2a cells to treatment with Tm.<sup>39</sup>

Dysregulation of the UPR in *Crelld2*-deficient livers is evident by increased expression of major UPR components, e.g., *Edem1*, *Ern1* (*Ire1*), and *Hspa5* upon Tm treatment. At the same time, they show decreased expression of *Perk* and *Perk* downstream target genes, such as *Herpud1* and *Hspa1a*,<sup>14,51</sup> as well as *Syvn1*, which is induced by sXbp1, possibly in coordinated action with *Atf6*.<sup>52</sup> UPR dysregulation is accompanied by downregulated gene expression of important components for lipid transport and catabolism, energy metabolism, and insulin signaling, which reportedly results in an impaired ER stress response.<sup>20,53–55</sup> Thus, *Crelld2*-deficient livers show overactive UPR but cannot fully activate the gene expression programs of all three UPR branches. Since *Crelld2* expression is induced by the *Atf6* pathway, we hypothesized that *Crelld2* regulates the *Atf6* axis. In fact, a majority of highly induced UPR genes in *Crelld2*-deficient livers are *Atf6* target genes (*Calr*, *Pdia4*, *Pdia6*, *Hsp90b1*, *Hyo1*).<sup>14</sup> However, *Crelld2*<sup>eGFP/eGFP</sup> mice also display deficient induction of parts of the *Perk* and *Ire1* pathway on the transcriptional level, suggesting that *Crelld2* is involved in crosstalk between the three UPR axes.

In contrast to pharmacological ER stress challenge, *Crelld2*<sup>eGFP/eGFP</sup> mice fed with HFD display an ameliorated dietary-induced obesity phenotype, hinting towards another layer of *Crelld2* impact on organ function. In this model, *Crelld2*-deficient mice reveal lower body weights and reduced liver steatosis. These findings are accompanied by the downregulated expression of genes important for lipid localization and transport but increased expression of genes necessary for lipid catabolism, a process required for energy production from fatty acids. These observations indicate that *Crelld2*<sup>eGFP/eGFP</sup> mice have a fundamentally higher energy expenditure. The underlying cause for the higher energy demand might be the upregulated expression of ribosomal genes, especially during HFD recovery (HFD > CD). Since the production of ribosomal proteins is a highly energy-consuming process,<sup>56</sup> *Crelld2*-deficient mice may upregulate ATP synthesis and, therefore, increase



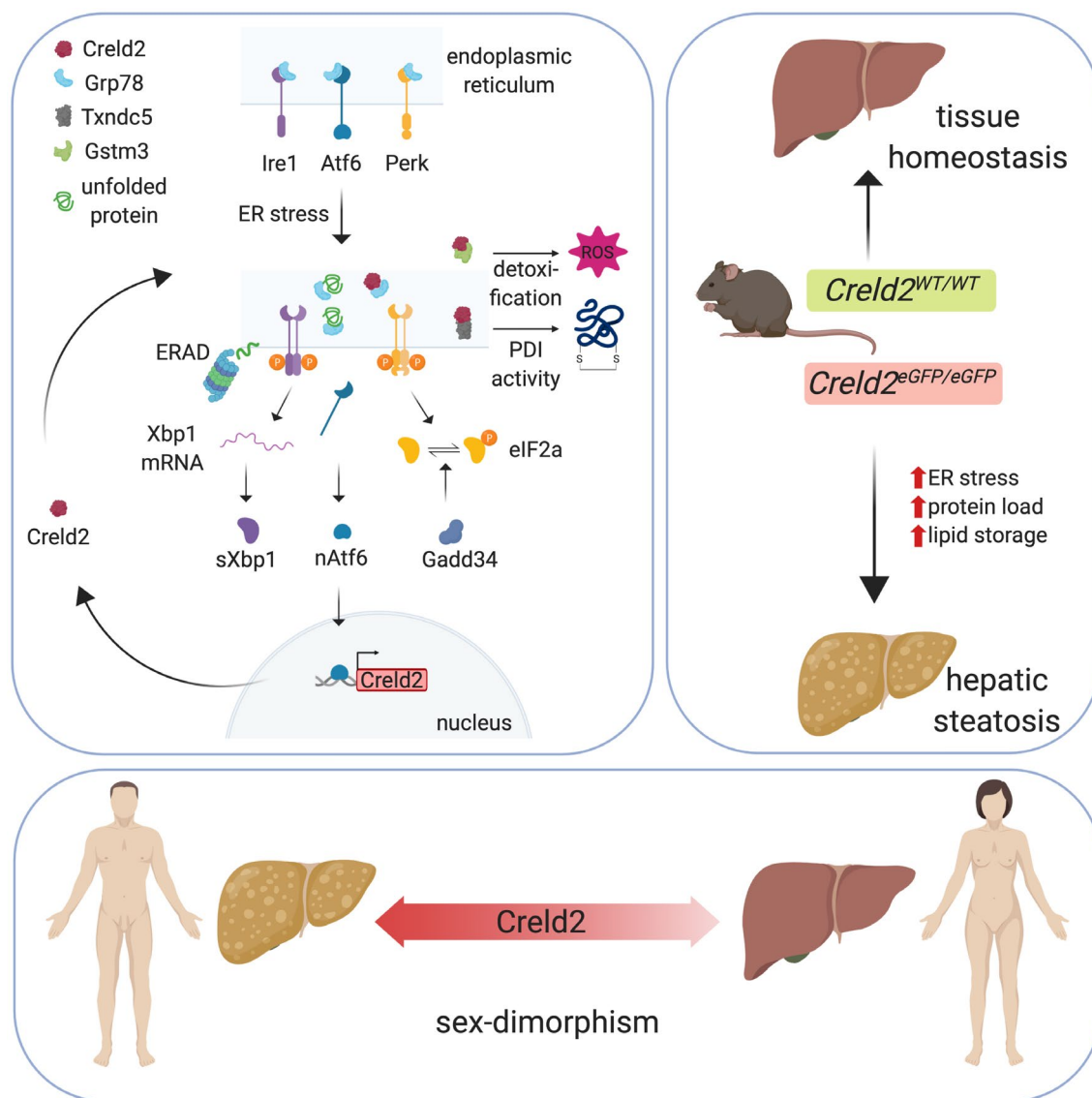


**FIGURE 7** Graphical summary of Creld2 function. Summary of Creld2 functionality, PDI, protein disulfide isomerase; ROS, reactive oxygen species. Created with BioRender.com

the utility and catabolism of lipids leading to the lower body weights and less accumulation of lipids in their livers as compared to littermate controls. Concomitantly, livers of Creld2<sup>eGFP/eGFP</sup> animals display reduced gene expression of UPR components in all conditions with the lowest induction during HFD recovery. These observations can be linked to previous reports showing that perturbation of Perk downstream components, eIF2α<sup>57</sup> or Atf4,<sup>58</sup> leads to diminished hepatosteatosis during HFD and leaner mice exhibiting increased energy expenditure, respectively. In addition, Perk inhibits the expression of ribosomal genes,<sup>51</sup> hinting toward impairment of Perk downstream signaling in Creld2-deficient mice. In turn, this might result in the upregulation of ribosomal genes followed by increased fatty acid catabolism for ATP production due to the increased energy demand in these mice.

Furthermore, we found no evidence that lipid accumulation through HFD per se induces UPR in wildtype or Creld2<sup>eGFP/eGFP</sup> livers. However, livers from Creld2<sup>eGFP/eGFP</sup> animals show first signs of cellular stress and apoptosis when compared to controls, which underlines the UPR-independent protective function of Creld2 upon oxidative stress and ceramide-mediated hepatotoxicity caused by HFD.<sup>59,60</sup> Further, the diet switch from HFD to CD did not promote ER-stress induction in both genotypes but instead reduced the expression of chaperones in Creld2<sup>eGFP/eGFP</sup> livers. Thus, we conclude that in our model of a 12-week 60 kJ% lard-based diet, UPR does not play a major role during diet-induced hepatic steatosis as long as this pathophysiology is reversible and did not progress to NASH. Taken together, our data support the hypothesis that Creld2 is required to protect cells against ongoing stress,

although the cells retain the ability to partially compensate through other signaling pathways.

Analysis of Creld2 interaction partners further implicates an active role in regulating the UPR: Creld2 protein accumulates 48 h after induced ER stress and has the capacity to bind to Grp78. This, in turn, may have two effects (i) Grp78 would be sequestered from Perk/Ire1/Atf6, and thereby these sensors would be activated, or (ii) Creld2 might act as a co-chaperone and aid Grp78 in protein folding. Further, Creld2 binds to the endo PDI Txnrc5 and glutathione S-transferase Gstm3, two proteins important for ER stress reduction<sup>61,62</sup> and ROS detoxification,<sup>63</sup> respectively. Txnrc5 was reported to be transcriptionally regulated by Atf6 and sXbp1,<sup>42</sup> which places Creld2 function at the intersection between protein folding processes and the three UPR axes. How binding to Creld2 influences the function of these proteins remains to be investigated. Nevertheless, based on our mouse work, we hypothesize that Creld2 has a dual role during steady-state and cellular stress conditions: it maintains balanced basal and ER stress-induced UPR activation, probably by modulating the Perk- and Atf6-dependent axes through binding to Grp78. At the same time, Creld2 might reduce misfolded proteins either through its own putative PDI activity or by promoting the PDI activity of Txnrc5 and the detoxification function of Gstm3.

Finally, we observed a sex dimorphism in aged mice, with only *Creld2*<sup>eGFP/eGFP</sup> males developing steatosis. This hints towards a Creld2-dependent mechanism required during long-lasting unresolved or subthreshold ER stress in secretory organs such as the liver. Sex differences in fatty liver diseases have been demonstrated in rodent models and human disease.<sup>64</sup> NAFLD is more prevalent in men and postmenopausal women than in premenopausal women, mainly attributed to hormone homeostasis and visceral fat accumulation.<sup>64,65</sup> However, we did not observe general obesity or increased fat accumulation outside the liver in aged male *Creld2*<sup>eGFP/eGFP</sup> mice (not shown). Therefore, we favor the hypothesis that the hepatic ER stress response is sex-dependent and, thus, a risk factor for developing NAFLD and progression to NASH or hepatocellular carcinoma (HCC), particularly in males. This is in line with our results showing that CRELD2 accumulates only in livers of male NASH patients, as well as a previous study demonstrating that kidneys of male mice are more susceptible to ER stress-induced acute kidney injury than those of females due to a testosterone-dependent mechanism.<sup>47</sup> Furthermore, CRELD2—among six other proteins that maintain ER homeostasis—was identified as an adverse prognostic biomarker for overall survival in HCC patients,<sup>66</sup> underlining that elevated and unresolved ER stress can promote liver pathophysiology. Therefore, it will be essential to take sexual dimorphism into account

in the future when studying the contribution of ER stress to hepatic steatosis as well as in the course of NAFLD treatment with UPR modulating agents.

## ACKNOWLEDGMENTS

The authors thank Prof. Michael Hoch for his long-standing support of this project, Thomas D. Rutkowski for feedback on the manuscript, Melanie Thielisch for technical support, and Dr Joachim Degen for help with the generation of *Creld2*<sup>eGFP/eGFP</sup> mice. The authors also thank Prof. Margarete Odenthal (Institute for Pathology, University Hospital Cologne), Prof. Hideo A. Baba und Martin Schlattjan (Institute for Pathology, University Hospital Essen), and Prof. Johannes Haybäck (Institute for Pathology, University Hospital Magdeburg) for histological preparation and assessments for the validation cohort. Additionally, the authors thank Prof. Niedergethmann (Department for General- and Visceral Surgery, Alfried Krupp Hospital, Essen, Germany) and Prof. Hasenberg (Helios Hospital Niederberg) for sample collection of the validation cohort. AC was funded by the DFG CA267/14-1. EM, EK, and JLS were funded by the DFG under Germany's Excellence Strategy EXC2151-390873048. JLS was funded by the BMBF competence cluster DietBB (01EA1809A). EM is supported by the Daimler and Benz Foundation. This work was funded by the Fritz Thyssen foundation (to EM, Az.10.18.2.029MN).

## DISCLOSURES

The authors declare no competing interests.

## AUTHOR CONTRIBUTIONS

Elvira Mass and Paul Kern conceived the project. Paul Kern, Elvira Mass, Nora R. Balzer, Klaus Wunderling, Nelli Blank, Cornelia Cygon, Alex Frolov, Lorenzo Bonaguro, and Franziska Bender performed experiments. Mirka Homrich and Eva Kiermaier supported WB experiments. Paul Kern, Elvira Mass, Nora R. Balzer, Nelli Blank, Cornelia Cygon, and Alex Frolov analyzed data. Elvira Mass, Paul Kern, Christoph Thiele, and Reinhard Bauer supervised experiments and data analysis. Thomas Ulas and Joachim L. Schultze provided help with RNA-seq experiments and the script for CoCena<sup>2</sup> analyses. Christoph Thiele helped with lipidomic analyses. Jan-Peter Sowa and Ali Canbay assisted in interpretation of human results. Elvira Mass and Paul Kern wrote the manuscript.

## DATA AVAILABILITY STATEMENT

Gene expression data are deposited at the GEO database (GSE143185). Original blots for Western Blots shown in Figure 1B (<https://doi.org/10.6084/m9.figshare.16530759.v1>) and Western Blot data for data quantified in Figure 2H and Figure 6D (<https://doi.org/10.6084/m9.figshare.16406>

601.v1) are deposited at the figshare repository. Lipid mass spectrometry data are deposited in a Github repository (<https://github.com/maccabaeus/Creld2-lipid-mass-spectrometry.git>). The data that support the findings of this study are available from the corresponding author upon reasonable request.

## ORCID

Elvira Mass  <https://orcid.org/0000-0003-2318-2356>

## REFERENCES

- Rupp PA, Fouad GT, Egelston CA, et al. Identification, genomic organization and mRNA expression of CRELD1, the founding member of a unique family of matricellular proteins. *Gene*. 2002;293:47-57.
- D'Alessandro M, Richard M, Stigloher C, et al. CRELD1 is an evolutionarily-conserved maturational enhancer of ionotropic acetylcholine receptors. *eLife*. 2018;7:e39649.
- Oh-hashii K, Kunieda R, Hirata Y, Kiuchi K. Biosynthesis and secretion of mouse cysteine-rich with EGF-like domains 2. *FEBS Lett*. 2011;585:2481-2487.
- Bonaguro L, Köhne M, Schmidleithner L, et al. CRELD1 modulates homeostasis of the immune system in mice and humans. *Nat Immunol*. 2020;21:1517-1527.
- Mass E, Wachten D, Aschenbrenner AC, Voelzmann A, Hoch M. Murine Creld1 controls cardiac development through activation of calcineurin/NFATc1 signaling. *Dev Cell*. 2014;28:711-726.
- Beckert V, Rassmann S, Kayvanjoo AH, et al. Creld1 regulates myocardial development and function. *J Mol Cell Cardiol*. 2021;156:45-56.
- Hartley CL, Edwards S, Mullan L, et al. Armet/Manf and Creld2 are components of a specialized ER stress response provoked by inappropriate formation of disulphide bonds: implications for genetic skeletal diseases. *Hum Mol Genet*. 2013;22:5262-5275.
- Boyle ST, Poltavets V, Kular J, et al. ROCK-mediated selective activation of PERK signalling causes fibroblast reprogramming and tumour progression through a CRELD2-dependent mechanism. *Nat Cell Biol*. 2020;22:882-895.
- Kim Y, Park S-J, Manson SR, et al. Elevated urinary CRELD2 is associated with endoplasmic reticulum stress-mediated kidney disease. *JCI Insight*. 2017;2:e92896.
- Chen M-F, Chang C-H, Yang L-Y, et al. Synovial fluid interleukin-16, interleukin-18, and CRELD2 as novel biomarkers of prosthetic joint infections. *Bone Joint Res*. 2019;8:179-188.
- Oh-hashii K, Koga H, Ikeda S, Shimada K, Hirata Y, Kiuchi K. CRELD2 is a novel endoplasmic reticulum stress-inducible gene. *Biochem Biophys Res Comm*. 2009;387:504-510.
- Oh-Hashi K, Koga H, Ikeda S, Shimada K, Hirata Y, Kiuchi K. Role of an ER stress response element in regulating the bidirectional promoter of the mouse CRELD2—ALG12 gene pair. *BMC Genom*. 2010;11:664.
- Adachi Y, Yamamoto K, Okada T, Yoshida H, Harada A, Mori K. ATF6 is a transcription factor specializing in the regulation of quality control proteins in the endoplasmic reticulum. *Cell Struct Funct*. 2008;33:75-89.
- Adamson B, Norman TM, Jost M, et al. A multiplexed single-cell CRISPR screening platform enables systematic dissection of the unfolded protein response. *Cell*. 2016;167:1867-1882.e21.
- Walter P, Ron D. The unfolded protein response: from stress pathway to homeostatic regulation. *Science*. 2011;334:1081-1086.
- Hetz C. The unfolded protein response: controlling cell fate decisions under ER stress and beyond. *Nat Rev Mol Cell Biol*. 2012;13:89-102.
- Song MJ, Malhi H. The unfolded protein response and hepatic lipid metabolism in non alcoholic fatty liver disease. *Pharmacol Ther*. 2019;203:107401.
- Hatahet F, Ruddock LW. Substrate recognition by the protein disulfide isomerases. *FEBS J*. 2007;274:5223-5234.
- Dennis EP, Edwards SM, Jackson RM, et al. CRELD2 is a novel LRP1 chaperone that regulates noncanonical WNT signaling in skeletal development. *J Bone Miner Res*. 2020;35:1452-1469.
- Rutkowski DT, Wu J, Back S-H, et al. UPR pathways combine to prevent hepatic steatosis caused by ER stress-mediated suppression of transcriptional master regulators. *Dev Cell*. 2008;15:829-840.
- Yamamoto K, Takahara K, Oyadomari S, et al. Induction of liver steatosis and lipid droplet formation in ATF6 $\alpha$ -knockout mice burdened with pharmacological endoplasmic reticulum stress. *Mol Biol Cell*. 2010;21:2975-2986.
- DeZwaan-McCabe D, Sheldon RD, Gorecki MC, et al. ER stress inhibits liver fatty acid oxidation while unmitigated stress leads to anorexia-induced lipolysis and both liver and kidney steatosis. *Cell Rep*. 2017;19:1794-1806.
- Fu S, Yang L, Li P, et al. Aberrant lipid metabolism disrupts calcium homeostasis causing liver endoplasmic reticulum stress in obesity. *Nature*. 2011;473:528-531.
- Ozcan U, Cao Q, Yilmaz E, et al. Endoplasmic reticulum stress links obesity, insulin action, and type 2 diabetes. *Science*. 2004;306:457-461.
- Ozcan U, Yilmaz E, Ozcan L, et al. Chemical chaperones reduce ER stress and restore glucose homeostasis in a mouse model of type 2 diabetes. *Science*. 2006;313:1137-1140.
- Kammoun HL, Chabanon H, Hainault I, et al. GRP78 expression inhibits insulin and ER stress-induced SREBP-1c activation and reduces hepatic steatosis in mice. *J Clin Invest*. 2009;119:1201-1215.
- Wu J, Rutkowski DT, Dubois M, et al. ATF6 $\alpha$  optimizes long-term endoplasmic reticulum function to protect cells from chronic stress. *Dev Cell*. 2007;13:351-364.
- Usui M, Yamaguchi S, Tanji Y, et al. Atf6 $\alpha$ -null mice are glucose intolerant due to pancreatic  $\beta$ -cell failure on a high-fat diet but partially resistant to diet-induced insulin resistance. *Metabolism*. 2012;61:1118-1128.
- Matthews DR, Hosker JP, Rudenski AS, Naylor BA, Treacher DF, Turner RC. Homeostasis model assessment: insulin resistance and beta-cell function from fasting plasma glucose and insulin concentrations in man. *Diabetologia*. 1985;28:412-419.
- Picelli S, Bjorklund AK, Faridani OR, Sagasser S, Winberg G, Sandberg R. Smart-seq2 for sensitive full-length transcriptome profiling in single cells. *Nat Methods*. 2013;10:1096-1098.
- Bray NL, Pimentel H, Melsted P, Pachter L. Near-optimal probabilistic RNA-seq quantification. *Nat Biotechnol*. 2016;34:525-527.
- Love MI, Huber W, Anders S. Moderated estimation of fold change and dispersion for RNA-seq data with DESeq2. *Genome Biol*. 2014;15:550.
- Leek J, Johnson W, Parker H, et al. sva: Surrogate Variable Analysis. R package version 3.34.0; 2019.



34. Blondel VD, Guillaume JL, Lambiotte R, Lefebvre E. Fast unfolding of communities in large networks. *J Stat Mech Theory Exp*. 2008;2008:P10008.
35. Rosvall M, Bergstrom CT. Maps of random walks on complex networks reveal community structure. *Proc Natl Acad Sci U S A*. 2008;105:1118-1123.
36. Yu G, Wang LG, Han Y, He QY. clusterProfiler: an R package for comparing biological themes among gene clusters. *OMICS*. 2012;16:284-287.
37. Bligh EG, Dyer WJ. A rapid method of total lipid extraction and purification. *Can J Biochem Physiol*. 1959;37:911-917.
38. Bedossa P, Poitou C, Veyrie N, et al. Histopathological algorithm and scoring system for evaluation of liver lesions in morbidly obese patients. *Hepatology*. 2012;56:1751-1759.
39. Oh-Hashi K, Fujimura K, Norisada J, Hirata Y. Expression analysis and functional characterization of the mouse cysteine-rich with EGF-like domains 2. *Sci Rep*. 2018;8:12236.
40. Kuipers EJ, Yang VW, Musso G, Cassader M, Paschetta E, Gambino R. REVIEWS IN BASIC AND CLINICAL GASTROENTEROLOGY AND HEPATOLOGY Bioactive lipid species and metabolic pathways in progression and resolution of nonalcoholic steatohepatitis. *Gastroenterology*. 2018;155:282-302.e8.
41. Gloeckner CJ, Boldt K, Schumacher A, Ueffing M. Tandem affinity purification of protein complexes from mammalian cells by the Strep/FLAG (SF)-TAP tag. *Methods Mol Biol*. 2009;564:359-372.
42. Horna-Terrón E, Pradilla-Dieste A, Sánchez-de-Diego C, Osada J. TXNDC5, a newly discovered disulfide isomerase with a key role in cell physiology and pathology. *Int J Mol Sci*. 2014;15:23501-23518.
43. Board PG, Menon D. Glutathione transferases, regulators of cellular metabolism and physiology. *Biochim Biophys Acta*. 2013;1830:3267-3288.
44. Zhang Z, Zhang L, Zhou L, Lei Y, Zhang Y, Huang C. Redox signaling and unfolded protein response coordinate cell fate decisions under ER stress. *Redox Biol*. 2019;25:101047.
45. Sheedfar F, Biase SD, Koonen D, Vinciguerra M. Liver diseases and aging: friends or foes? *Aging Cell*. 2013;12:950-954.
46. Pibiri M. Liver regeneration in aged mice: new insights. *Aging*. 2018;10:1801-1824.
47. Hodeify R, Megyesi J, Tarcsfalvi A, Mustafa HI, Seng HL, Hti Lar Seng NS, Price PM. Gender differences control the susceptibility to ER stress-induced acute kidney injury. *Am J Physiol Renal Physiol*. 2013;304:F875-F882.
48. Palmisano BT, Stafford JM, Pendergast JS. High-fat feeding does not disrupt daily rhythms in female mice because of protection by ovarian hormones. *Front Endocrinol*. 2017;8:14.
49. Medrikova D, Jilkova ZM, Bardova K, Janovska P, Rossmeisl M, Kopecky J. Sex differences during the course of diet-induced obesity in mice: adipose tissue expandability and glycemic control. *Int J Obes*. 2012;2005(36):262-272.
50. Lefere S, Tacke F. Macrophages in obesity and non-alcoholic fatty liver disease: crosstalk with metabolism. *JHEP Rep*. 2019;1:30-43.
51. Gonen N, Sabath N, Burge CB, Shalgi R. Widespread PERK-dependent repression of ER targets in response to ER stress. *Sci Rep*. 2019;9:1-12.
52. Savic S, Ouboussad L, Dickie LJ, et al. TLR dependent XBP-1 activation induces an autocrine loop in rheumatoid arthritis synoviocytes. *J Autoimmun*. 2014;50:59-66.
53. Han J, Kaufman RJ. The role of ER stress in lipid metabolism and lipotoxicity. *J Lipid Res*. 2016;57:1329-1338.
54. Malhi H, Kaufman RJ. Endoplasmic reticulum stress in liver disease. *J Hepatol*. 2011;54:795-809.
55. Zhang K, Wang S, Malhotra J, et al. The unfolded protein response transducer IRE1 $\alpha$  prevents ER stress-induced hepatic steatosis. *EMBO J*. 2011;30:1357-1375.
56. Strunk BS, Karbstein K. Powering through ribosome assembly. *RNA*. 2009;15:2083-2104.
57. Oyadomari S, Harding HP, Zhang Y, Oyadomari M, Ron D. Dephosphorylation of translation initiation factor 2 $\alpha$  enhances glucose tolerance and attenuates hepatosteatosis in mice. *Cell Metab*. 2008;7:520-532.
58. Wang C, Huang Z, Du Y, Cheng Y, Chen S, Guo F. ATF4 regulates lipid metabolism and thermogenesis. *Cell Res*. 2010;20:174-184.
59. Longato L, Tong M, Wands JR, de la Monte SM. High fat diet induced hepatic steatosis and insulin resistance: role of dysregulated ceramide metabolism. *Hepatol Res*. 2012;42:412-427.
60. Kurek K, Piotrowska DM, Wiesiolek-Kurek P, et al. Inhibition of ceramide de novo synthesis reduces liver lipid accumulation in rats with nonalcoholic fatty liver disease. *Liver Int*. 2014;34:1074-1083.
61. Alberti A, Karamessinis P, Peroulis M, et al. ERp46 is reduced by high glucose and regulates insulin content in pancreatic  $\beta$ -cells. *Am J Physiol Endocrinol Metab*. 2009;297:E812-E821.
62. Chen DL, Xiang JN, Yang LY. Role of ERp46 in  $\beta$ -cell lipoapoptosis through endoplasmic reticulum stress pathway as well as the protective effect of exendin-4. *Biochem Biophys Res Comm*. 2012;426:324-329.
63. Wang S, Yang J, Ding C, et al. Glutathione S-transferase Mu-3 predicts a better prognosis and inhibits malignant behavior and glycolysis in pancreatic cancer. *Front Oncol*. 2020;10:1539.
64. Ballestri S, Nascimbeni F, Baldelli E, Marrazzo A, Romagnoli D, Lonardo A. NAFLD as a sexual dimorphic disease: role of gender and reproductive status in the development and progression of nonalcoholic fatty liver disease and inherent cardiovascular risk. *Adv Ther*. 2017;34:1291-1326.
65. Lonardo A, Suzuki A. Nonalcoholic fatty liver disease: does sex matter? *Hepatobiliary Surg Nutr*. 2019;8:164-166.
66. Liu G-M, Zeng H-D, Zhang C-Y, Xu J-W. Key genes associated with diabetes mellitus and hepatocellular carcinoma. *Pathol Res Pract*. 2019;215:152510.

## SUPPORTING INFORMATION

Additional Supporting Information may be found in the online version of the article at the publisher's website.

**How to cite this article:** Kern P, Balzer NR, Blank N, et al. Creld2 function during unfolded protein response is essential for liver metabolism homeostasis. *FASEB J*. 2021;35:e21939. doi:[10.1096/fj.202002713RR](https://doi.org/10.1096/fj.202002713RR)